16

Structural and Dynamic Basis of Serine Proteases from Nematophagous Fungi for Cuticle Degradation

Shu-Qun Liu[1,2], Lian-Ming Liang[1], Tao Yan[1], Li-Quan Yang[1], Xing-Lai Ji[1,2], Jin-Kui Yang[1], Yun-Xin Fu[1,3] and Ke-Qin Zhang[1]
[1]Laboratory for Conservation and Utilization of Bio-Resources & Key Laboratory for Microbial Resources of the Ministry of Education, Yunnan University, Kunming,
[2]Sino-Dutch Biomedial and Information Engineering School, Northeastern University, Shenyang
[3]Human Genetics Center, School of Public Health, The University of Texas Health Science Center, Houston, Texas,
[1,2]P. R. China
[3]USA

1. Introduction

Serine proteases derived from nematophagous fungi are known as one of the most important virulence determinants during infection processes due to their ability to degrade nematode cuticle, a hard physical barrier protecting nematodes from physical damage or pathogen infections. Understanding the structural and dynamic features of cuticle-degrading serine proteases is fundamental to uncovering and describing the mechanism of nematicide by fungi at molecular level, which in turn will facilitate protein engineering study aimed at improving nematicidal activity of fungi.

In this chapter we describe several three-dimensional structural models of cuticle-degrading serine proteases secreted by different nematophagous fungi. The atomic coordinates of these models were obtained using methods such as the protein comparative modeling or the X-ray crystallography. Detailed comparison between these structures shows that, despite their striking degree of structural similarity, there are subtle differences in size, shape and hydrophathy of substrate-binding pockets S1 and S4 caused by single or multiple amino acid substitutions within the substrate-binding region. This explains why these enzymes have different substrate specificity and catalytic efficiency. Moreover, the amino acid changes in substrate-binding region and in overall enzyme molecule give rise to distinctly different electrostatic surface potential distribution among these proteases, possibly contributing to the distinct ability to attract the nematode cuticle with overall dominantly electronegative charge. The dynamic structural features of a classical serine protease

Shu-Qun Liu & Lian-Ming Liang contribute equally to this work
Corresponding author e-mail: kqzhang1@yahoo.com.cn

proteinase K (PRK) were also investigated using molecular dynamics (MD) simulation technique. The different degree of flexibility of the substrate binding region was proposed to be linked to different substrate affinity and catalytic activity of these proteases; the first few modes of motions of substrate-binding pockets S1-S4, which were obtained using essential dynamics analysis, were proposed to be related to detailed dynamic progresses including substrate binding, positioning, catalysis, and product release.

The difference in thermal stability and nematicidal/catalytic activity between the alkaline serine proteases secreted by nematode-parasitic fungi and neutral proteases derived from nematode-trapping fungi can be attributed to the difference in global structural rigidity and local conformational flexibility (i.e., within the active site) caused by the presence/absence of disulfide bonds in the alkaline/neutral proteases. Of particular interest is that the nematode-parasitic and nematode-trapping fungi have evolved to adopt different strategies to obtain nutrient, i.e., the nematode-parasitic fungi, although have no trap device, produce powerful alkaline proteases (which carry predominant electro-positive surface potential) to diffuse towards and degrade hosts effectively, whereas the nematode-trapping fungi produce neutral proteases that carry predominant electro-negative surface potential and exhibit relatively weak catalytic activity, which can be compensated for by the active prey catch using their trap devices.

Taken together, the differences in dynamic behavior of substrate-binding region between cuticle-degrading proteases, in conjunction with differences in electrostatic surface potential distribution of these enzyme molecules and in architecture and hydrophathic property of substrate-binding pockets, could be used to explain their different catalytic activities towards nematode cuticle, thus facilitating in turn the explanation for different nematicidal activities by different fungi. The structures and dynamics of these cuticle-degrading serine proteases provide a solid basis for exploiting these enzymes from nematicidal fungi as effective bio-control agents.

2. Plant-parasitic nematodes and relevant control strategies

2.1 Description of the plant-parasitic nematodes

Nematodes are unsegmented roundworms and those that attack and parasitize plant are called plant-parasitic nematodes, which are a very important group of agricultural pests. Although the damage the plant-parasitic nematodes cause to plants is often subtle and is easily confused with nutrient problems, their enormous population numbers and broad plant host range can cause very serious damage to farmers and agricultural production, as indicated by the annual loss estimates of >100 billion US dollars throughout the world (Sasser & Freekman, 1987).

Plant nematodes are tiny worms whose body is covered by transparent and colorless cuticle, body length ranges from 0.25 mm to 3 mm and body shape is cylindrical, tapering toward the head and tail. The life cycle of a plant-parasitic nematode has six stages and four molts, i.e., egg, four juvenile stages and adult separated by molts (J1 - M1 - J2 - (Hatch) - M2 - J3- M3 - J4 - M4 - Adult). The first molt (M1) occurs in the egg between the first-stage juvenile (J1) and second-stage juvenile (J2); the emerging J2 is the most common infective stage; and the length of life cycle of plant parasitic nematodes can be anywhere from 20-40 days (on average 25 days at 22 ^{o}C) (Snyder, 2002). Plant parasitic nematodes, whether root-feeders or foliage-feeders, have a spear-like mouthpart that is able to puncture effectively host cells

and feed on the cell contents. Such a feeding, accompanied by injection of some enzymes and toxins into the host cell by nematodes, causes abnormal plant growth, and consequently the plants can be stunted, discolored, or both (Schmitt & Sipes, 1998).

2.2 Nematode control strategies and biological control

The goal of nematode control is to manage their population and reduce their numbers below the damaging levels to plants due to the fact that the thorough elimination of nematodes is not possible. The principle of nematode management is multifaceted, and as a result many conventional methods have been developed including planting resistant crop varieties, rotating crops, incorporating soil amendments, and applying pesticides (Schmitt & Sipes, 1998). Although the management methods involving no pesticides are environmentally friendly, their applications usually fail to keep nematodes below damaging levels for reasons that these methods are all to some extent limited, specific, hard to operate, and of low efficiency. Applications of the chemical nematicides are usually more effective in reducing nematode numbers than traditional non-pesticide methods because of the direct killing action on nematodes. However, most chemical nematicides are highly toxic synthetic pesticides, which are environmentally risky and extremely dangerous to people and other animals if handled carelessly. On the other hand, the abuse of nematicides could induce widespread resistance in field populations of many plant nematodes.

Another interesting nematode control approach is the biological control - using other organisms, i.e., the natural enemies, against the pest organism. The natural enemies of nematodes, which are usually isolated from nematode populations and are able to keep the population of nematode at apparently low levels, are usually some bacteria and fungi called nematophagous bacteria and fungi. Nematophagous bacteria are groups of bacteria that exhibit diverse modes of actions on nematodes, such as emitting potent volatile organic compounds to lure nematodes (Niu et al., 2010), producing toxins to suppress host defense and alter cellular metabolism, and secreting enzymes to degrade host cuticle or intestinal tissue, leading to the parasitization of bacteria and subsequent death of nematodes (Lobna & Zawam, 2010; Tian et al., 2007). Nematophagous fungi are a diverse group of carnivorous fungal species that use their spores or mycelial structures to capture nematodes (which are called nematode-trapping fungi), or use their hyphal tips to parasitize the eggs and cysts of nematodes (Nordbring-Hertz, 2004), or produce toxins/enzymes to attack/degrade nematodes (which are called nematode-parasitic fungi) (T.F. Li et al., 2000; X.Z. Liu et al., 2009). Although under laboratory conditions some nematophagous bacteria and fungi have been shown to reduce populations of some kinds of nematodes, the successes at the full-scale field level have been limited (Schmitt & Sipes, 1998). The possible reasons for this are that i) most organisms that are recognized as biological control agents are highly host-specific, attacking just one or few of the nematode pests; ii) the nematophagous bacteria and fungi are too difficult to culture to obtain sufficient quantities that are useful for field application. Nevertheless, applying biological control as a means to reduce the harm of nematodes to agriculture production has always attracted considerable attention because of the apparent advantages of this method: i) the nematophagous microorganisms are nonpolluting and therefore environmentally acceptable and safe, and as such utilizing such agents can avoid the use of ecologically and environmentally hazardous chemicals, promoting the ecological balance; ii) biological control is considered to be more effective against agricultural pests that are less harmful, that only need to be controlled and

suppressed and can not be permanently eliminated (i.e., the nematode) (Writing, 2011), and therefore the utilization of nematophagous microorganisms is beneficial to increasing biodiversity in soil; iii) biological control has potentially huge economic and commercial value and simultaneously its relevant research, development and application will provide many employment and job opportunities.

During the past decades, the nematode-targeted biological control study is mainly focused on elucidating the pathogenic/infection mechanism of nematophagous microorganisms since this is essential for developing effective biological control agents against nematodes. For example, a "Trojan horse" mechanism of a nematophagous bacterium, *Bacillus nematocida* B16, against nematodes has been reported recently by our lab (Niu et al., 2010), indicating that this bacterium can lure nematodes that are relatively distant to move close to the bacteria through producing volatile organic compounds; and the subsequent uptake of bacteria as food by nematode offers the opportunity for bacteria to secrete proteases with broad substrate specificity to degrade the intestinal wall of nematode. We also sequenced the whole genome of the nematode-trapping fungus *Arthrobotrys oligospora* Fres. (ATCC 24927) to reveal genes likely involved in pathogenesis of this nematophagous fungus; the subsequent proteomic and RT-PCR analyses of protein differential expression induced by the presence of nematode extract revealed that many cellular processes such as energy metabolism, biosynthesis of the cell wall and adhesive proteins, cell division, glycerol accumulation and peroxisome biogenesis, determine, participate in and regulate the formation of the trap device (J. K. Yang et al., 2011). The analysis of the *A. oligospora* genome revealed that this nematophagous species has a larger number of enzyme genes such as those encoding the enzyme families of subtilisin, collagenase, pectinesterase and pectate lyase in comparison with several sequenced model ascomycete fungi (J. K. Yang et al., 2011).

2.3 Nematode cuticle, its components and cuticle-degrading enzymes

Like the majority of pathogens that infect/attack the hosts, the fist step of the infection by nematophagous fungi is to break open the cuticle of the host followed by pathogens entry. The cuticle is a multi-functional exoskeleton and is a highly impervious barrier between the animal (such as nematode and insect) and its environment. Cuticle is also essential for the maintenance of body morphology and integrity, and simultaneously plays a critical role in locomotion via attachments to body-wall muscles (Page & Johnstone, 2007). Since the main structural components of the nematode cuticle are proteins, highly cross-linked collagens, chitin fibrils and specialized insoluble proteins known as "cuticlins", together with glycoproteins and lipids (Page & Johnstone, 2007), it is not surprising that nematophagous fungi need to produce a variety of highly efficient enzymes such as proteases, collagenases, chitinases and lipases to act together to degrade the first defense line - the cuticle of the nematode. Among the above-mentioned enzymes, the proteases are considered to be most important during infection since the protein matrix is the most important component of the nematode cuticle and the quantity and type of proteins vary between species, tissues and growth stages of nematodes (Huang et al., 2004; Jansson & Nordbring-Hertz, 1988).

During the past several years, several cuticle-degrading proteases have been purified and characterized from different nematophagous or entomopathogenic fungi such as *Arthrobotrys oligospora* (Tunlid et al., 1994; Zhao et al., 2004), *Pochonia chlamydospora* (syn. *Verticillium chlamydosporium*) (R. Segers et al., 1994), *Beauveria bassiana* (Joshi et al., 1995), and

Metarhizium anisopliae (R.J. St Leger et al., 1987); and their catalytic activities towards casein and cuticle proteins were shown to be high, suggesting their highly nematicidal activities. Cloning and sequencing of the genes coding for these cuticle-degrading proteases (Joshi et al., 1995; R. Segers et al., 1994; R.J. St Leger et al., 1987; Tunlid et al., 1994; Zhao et al., 2004) reveal that these proteases have a high degree of sequence similarity to each other and to the proteinase K (EC 3.4.21.64) derived from *Tritirachium album* Limber (Ebeling et al., 1974), suggesting that these proteases belong to the proteinase K subfamily of the secretory subtilase/subtilisin-like serine protease family, known as the peptidase family S8 according to the classification and nomenclature of peptidases in the MEROPS database (Rawlings et al., 2010). This peptidase family is also the second largest family of serine peptidases, both in terms of number of sequences and characterized peptidases, and distributes broadly from viruses, bacteria, and fungi to plants and animals. Although the physiochemical properties, optimum reaction conditions, substrate specificity, catalytic mechanism, dynamics, and structure-function relationship of the representative enzyme of the peptidase S8 family, the proteinase K, have been extensively studied (Bajorath et al., 1989; Betzel et al., 2001; Betzel et al., 1988; Betzel et al., 1986; Betzel et al., 1993; Ebeling et al., 1974; Hilz et al., 1975; S. Q. Liu et al., 2010, 2011; Müller et al., 1994; Pahler et al., 1984; Tao et al., 2010; Wolf et al., 1991), a thorough understanding of the above characteristics for the cuticle-degrading serine proteases from nematophagous fungi is of crucial importance in uncovering and describing the nematicidal mechanism by fungi at molecular level. In this chapter we describe how the variation in amino acid sequence affect the functional properties (such as substrate specificity and catalytic efficiency) of the cuticle-degrading proteases derived from different fungi through comprehensive investigation into the three-dimensional structural models of these enzymes, which will facilitate the improvement in biological control potential of nematophagous fungi through protein engineering or site-directed mutagenesis.

3. Catalytic mechanism of serine proteases

Proteases are enzymes that break down protein through hydrolysis of the peptide bonds that link amino acids together in the polypeptide chain forming the protein. They occur naturally in all organisms and involve various physiological reactions from simple digestion of proteins in food to highly-regulated cascades. Proteases are currently divided into four major groups according to the character of their catalytic active site and conditions of action: serine proteinases, cysteine (thiol) proteinases, aspartic proteinases, and metalloproteinases. Classification of a protease into a certain group depends on the structure of catalytic site and the essential amino acid acting as a nucleophile. Accordingly, serine proteases (EC 3.4.21) are proteases in which one of the amino acids in the active site of the enzyme is the serine. This group of proteases is present in virtually all organisms and is further classified into two clans: the chymotrypsin-clan and the subtilisin-clan. These two clans are evolutionarily unrelated and have distinct overall folded structures but share the same catalytic mechanism utilizing an identical stereochemistry of the catalytic triad where the serine act as the nucleophile (Blow, 1976; Siezen et al., 1991; Siezen & Leunissen, 1997; Tsukuda & Blow, 1985). This has been regarded as a classic example to illustrate convergent evolution showing the same catalytic mechanism evolved twice independently during evolution. The catalytic triad, located at the active site of protease, is a coordinated structure consisting of three essential amino acids: aspartic acid (Asp39 in proteinase K numbering; hereafter, all

numbering uses proteinase K as reference), histidine (His69), and serine (Ser224). These three key amino acid residues are located adjacent to one another near the heart of the enzyme (Figure 1), each playing an essential role in the cleaving process of the peptide bond (Birktoft & Blow, 1972; Dodson & Wlodawer, 1998; Kraut, 1977; Russell & Fersht, 1987):

- The Ser uses its hydroxyl group (-OH) as the primary nucleophile, which is able to attack the carbonyl carbon (C=O) of the scissile peptide bond (-C(=O)NH-) of the substrate.
- The His plays a dual role as the proton donor and acceptor at different steps in the reaction, i.e., a pair of electrons on the His nitrogen has the ability to accept the hydrogen from the serine hydroxyl group, thus coordinating the attack of the peptide bond.
- The role of Asp is believed to bring the His into the correct orientation by its carboxyl group hydrogen bonding with the His, thus facilitating the nucleophilic attack by the Ser.

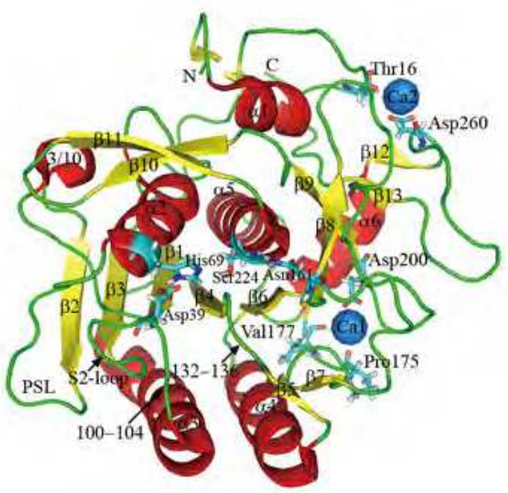

Fig. 1. Ribbon diagram of proteinase K (PDB code 1IC6). The α helices, β strands and loops/links are colored red, yellow and green, respectively. The residues of the catalytic triad (Asp39, His69 and Ser224), oxyanion hole (Asn161), and calcium binding sites (Ca1 site: Pro175, Val177 and Asp200; Ca2 site: Thr16 and Asp260) are shown as stick models with the carbon, nitrogen and oxygen colored cyan, blue and red, respectively. The two bound Ca^{2+} cations, Ca1 and Ca2, are shown as blue spheres. The secondary structure elements, substrate-binding regions of residues 100-104 and 132-132, polar surface loop (PSL loop) and S2-loop are labeled.

The detailed process of the catalytic mechanism can be described as follows (see also Figure 2):

1. After the binding of substrate and the positioning of scissile peptide bond is accomplished, the nitrogen atom of His accepts a hydrogen atom from the hydroxyl group of Ser, followed by a hydroxyl oxygen atom of Ser initiating the attack on the carbonyl carbon atom of the peptide bond, and the subsequent movement of a pair of electrons from the carbonyl double bond to the oxygen, resulting in the formation of a tetrahedral intermediate.
2. The covalent electrons creating the single peptide bond move to attack the hydrogen atom of His, resulting in the breaking of the peptide bond. The electrons on the negative

oxygen move back to recreate carbonyl oxygen double bond, producing an acyl-enzyme intermediate and a new N-terminus of the cleaved peptide chain.

3. A water molecule enters into the reaction through replacing the N-terminus of the cleaved peptide. It attacks the carbonyl carbon atom, followed by electrons moving from the double bond to the oxygen making it negative, resulting in the formation of a bond connecting the oxygen atom of the water and the carbonyl carbon atom. The His nitrogen atom accepts a proton from the water and coordinates the newly formed second tetrahedral intermediate via a hydrogen bond.
4. The final step involves the breaking of the bond formed in the first step between the Ser hydroxyl oxygen atom and the peptide bond carbonyl carbon atom. This is achieved via the attack of the His hydrogen (which is just acquired from the water) on this bond. The resultant electron-deficient carbonyl carbon reforms the double bond with the oxygen, resulting in the final release of the C-terminal product of the peptide.

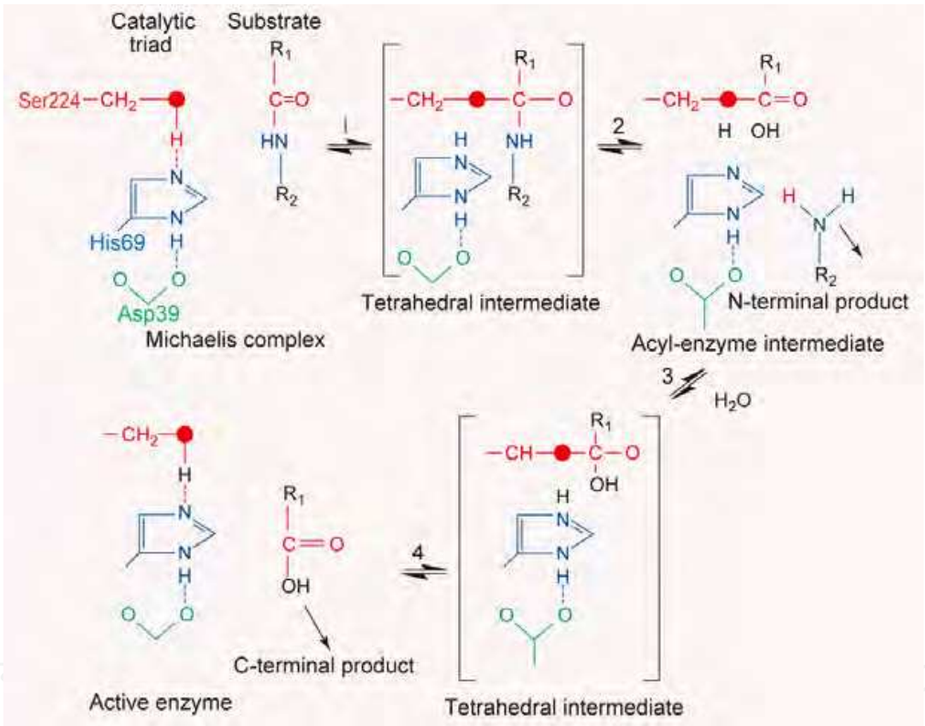

Fig. 2. Steps of the catalytic reaction by the catalytic triad of serine protease proteinase K. The nucleophile residue Ser is shown in red; the red dot indicates the nucleophilic atom hydroxyl oxygen. The His and Asp are shown in blue and green, respectively. This figure is modified from (Dodson & Wlodawer, 1998; Kraut, 1977); see text for details.

During the catalytic reaction process, the resultant negatively charged oxygen ion of the tetrahedral intermediate generated in steps 1 and 3 are believed to be stabilized by the so-called structural component of "oxyanion hole", which is formed by Ser224 (N), Asn161 (N), and Asn161 (N_δ), donating their backbone or side chain hydrogens to hydrogen bond with oxygen ion (Figure 1, 6D, E) (Betzel et al., 1986; Wolf et al., 1991). Like almost all other enzymes, the serine proteases can accelerate reaction because they bind the transition state (here is the tetrahedral intermediate) better than they bind either the Michaelis complex or

the acyl-enzyme intermediate, thus lowering the activation free energy barrier of the reaction.

4. Homology modeling of the cuticle-degrading proteases from fungi

In order to characterize the structural features and functional properties of cuticle-degrading serine proteases from fungi, we have built homology models of several proteases (S.Q. Liu et al., 2007b) based on the X-ray crystallographic structure of proteinase K (Betzel et al., 2001). These are PR1 (GenBank accession number AJ416695) from entomopathogenic fungus *Metarhizium anisopliae* (R.J. St Leger et al., 1987; R.J. St Leger et al., 1993), VCP1 (GenBank accession number AJ427460) from the nematophagous fungus, *Pochonia chlamydosporia* (Syn. *Verticillium chlamydosporium*) (Morton et al., 2003; R. Segers et al., 1996), Ver112 (GenBank accession number AY692148) from the nematophagous fungus *Lecanicillium psalliotae* (J.K. Yang et al., 2005a; J.K. Yang et al., 2005b), and PL646 (GenBank accession number EF094858) (Liang et al., 2010) from a saprobic, filamentous fungus *Paecilomyces lilacinus*, which is found to have a wide range of hosts such as nematodes (Jatala, 1986; Stirling & West, 1991), insects (Fiedler & Sosnowska, 2007; Rombach et al., 1986) and humans (Saberhagen et al., 1997; Westenfeld et al., 1996). *P. lilacinus* has been applied as a biocontrol agent to control the growth of destructive root-knot nematodes, resulting in several successful field trials on a range of crops in different soil types and climates (Jatala, 1986; Jatala et al., 1979). Of these proteases, PR1 is considered as a crucial factor in the infection of the insect in that it was detected with gold-labeled antibodies during the penetration of the insect cuticle by *Metarhizium anisopliae* (Goettel et al., 1989), and the rapid production and high concentration of this enzyme were also observed during infection (R.J. St Leger et al., 1986). The latter three are alkaline serine proteases which exhibit a crucial role in the penetration process of nematode eggs or cuticles.

4.1 Physiochemical properties and optimum reaction conditions

For these four cuticle-degrading proteases and proteinase K, their physiochemical properties were theoretically predicted (i.e., the programs SAPS (Brendel et al., 1992), EXTCOEF (Gill & von Hipple, 1989) and pI web server (Lehninger, 1995) were used for predicting the molecular weight, extinction coefficient (EXTCOEF) at 280 nm, and isoelectric point (pI), respectively) and the optimum reaction conditions were experimentally determined (S.Q. Liu et al., 2007b). The results (Table 1) show that many physiochemical properties among these enzymes are very similar to each other, i.e., the residue number ranges from 279 to 284 and molecular weight is between 28.5 and 28.9 kDa, pI is high with values greater than 7.7, EXTCOEF is comparable at 280 nm, and have common susceptivity to inhibitor PMSF. Enzyme kinetics assays with substrates such as Suc-Ala-Ala-Ala-p-nitroaniline, Suc-Ala-Ala-Pro-Phe-p-nitroaniline and casein showed that these enzymes exhibited almost the same optimum reaction conditions, i.e., the high catalytic efficiencies were found at pH 8-10 and temperatures 50-60 °C (Liang et al., 2010; R. Segers et al., 1996; R.J. St Leger et al., 1987; J.K. Yang et al., 2005b). These highly similar properties can be explained by the high degree of amino acid sequence identity (> 60%) among proteinase K, PR1, VCP1, Ver112 and PL646, suggesting that these five proteases are members of the proteinase K subfamily and all are alkaline serine proteases, in agreement with previous propositions.

In addition, we also used the soluble proteins extracted from *C. elegans* nematode cuticle as substrates to test catalytic efficiencies of Ver112, PL646 and proteinase K. The results

showed that the three proteases commonly had high catalytic activities towards cuticle extract at their optimum reaction conditions (Liang et al., 2010). These three proteases also exhibit similar relatively high catalytic activities towards collagen (Liang et al., 2010).

Protease	Fungus	Host	MW[a] (kDa)	NAA[b]	pI[c]	RK/ DE[d]	EXTCOEF[e] ($M^{-1}cm^{-1}$)	Inhibitor	SI[h] (%)	Optimum[i]	
										pH	T[j](°C)
PRK	*Tritirachium album*	Human	28.9	279	7.71	20/19	33200	PMSF[f] DFP[g]	100	7.5-12	50-60
PR1	*Metarhizium anisopliae*	Insect	28.6	281	8.37	21/18	26800	PMSF	66.4	8-10	50-60
VCP1	*Pochonia chlamydosporia*	Nematode	28.5	281	7.74	20/19	28650	PMSF	62.5	8-10	50-60
Ver112	*Lecanicillium psalliotae*	Insect	28.6	280	8.67	22/18	27370	PMSF	64.1	8-10	50-60
PL646	*Paecilomyces lilacinus*	Nematode /Insect/ Human	28.7	284	8.38	19/16	25760	PMSF	62.0	8-10	50-70

[a] Calculated molecular weight.
[b] Number of amino acids.
[c] Predicted isoelectric point.
[d] Number of positively charged residues/number of negatively charged residues.
[e] Predicted extinction coefficient at 280 nm.
[f] Phenyl methane sulphonyl fluoride.
[g] Diisopropyl fluorophosphates.
[h] Sequence identity with respect to 1IC6.
[i] Optimal reaction conditions.
[j] Temperature.

Table 1. Physiochemical properties and optimal reaction conditions of the proteinase K (PRK) and the four cuticle-degrading enzymes PR1, VCP1, Ver112 and PL646.

The reasons for these proteases exhibiting high catalytic activity at both high temperature and high pH may be explained as follows. The elevated temperature can enhance conformational flexibility of enzyme structures, especially in the substrate-binding regions with relatively few conformational restrictions, thus enhancing the substrate affinity and catalytic efficiency of these enzymes (Gudjonsdottir & Asgeirsson, 2008; S. Q. Liu et al., 2010, 2011; Tao et al., 2010). Because excessively high temperatures will lead to thermal denaturation of the protein structure, the temperature just below the transition temperature is often the optimal reaction temperature of these proteases. The relatively high pH value is beneficial for maintaining the correct hydrogen bonding interaction within the catalytic triad, i.e., the hydrogen bonds His-$N_{\delta1}$-H···$O_{\delta2}$-Asp and Ser-O_{γ}-H···$N_{\varepsilon2}$-His, via proper protonation state for one of the catalytic triad residues His, i.e., protonation on the $N_{\delta1}$ atom but not on $N_{\varepsilon2}$ atom in the imidazole group.

4.2 Description and comparison of structural models

The structural models of PR1, VCP1, Ver112 and PL646 were built based on the high-resolution crystal structure of proteinase K (0.98 Å; PDB code 1IC6; hereafter proteinase K is

also referred to as 1IC6) using homology modeling technique implemented in the software package MODELLER 7v7 (Sali & Blundell, 1993). Because of the high degree of sequence identity (> 60%) of these proteases with respect to their template 1IC6, especially in the loop regions (Figure 3), it is not surprising that these modeled structures are nearly identical, whether to each other or to the template (Figure 4). Commonly, these models show the common α/β scaffold characteristics of the subtilisin-like serine protease, which consist of six α helices, two 3/10 helices, a seven-stranded parallel β sheet, and three two-stranded antiparallel β sheets. The corresponding amino acid sequences of these secondary structure elements are also indicated at the top of the multiple sequence alignment plot (Figure 3).

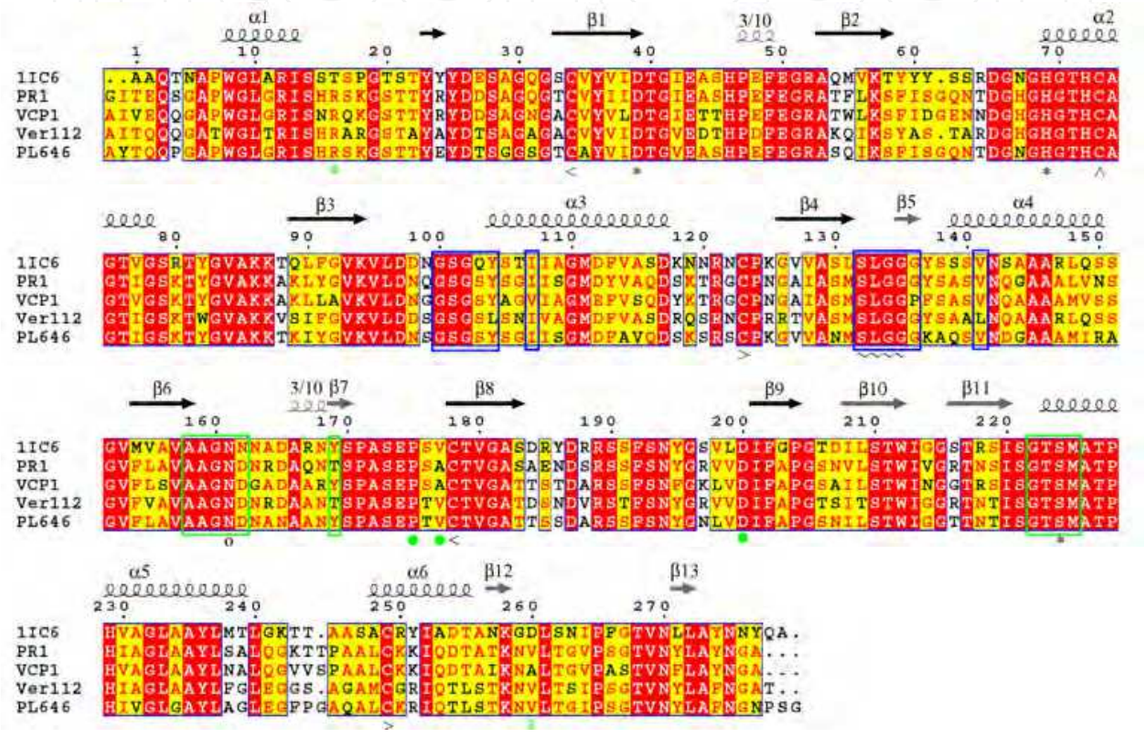

Fig. 3. Multiple sequence alignment of proteinase K (1IC6) and cuticle-degrading proteases PR1, VCP1, Ver112 and PL646. The regions of residues with red background and white foreground are completely conserved; those with yellow background and red foreground are well conserved or similar, and with black foreground are not conserved. The common secondary structure elements are indicated at the top with black arrows for parallel β strands, gray arrows for antiparallel β strands, black curves for α helices, and gray curves for 3/10 helices, respectively. Residues participating in the formation of the S1 site are circled by green frames, and those in the S4 site are circled by blue frames. ~ at the bottom indicates residues that participate in the formation of both S1 and S4 sites. Catalytic triad residues Asp39, His69 and Ser224 (proteinase K numbering) are marked at the bottom with a *. Oxyanion hole residue Asn161 is marked with o. Cysteines involved in the disulfide bridges are marked with < and > (<Cys34-Cys123> and <Cys178-Cys249>). The free Cys73 is with ∧. Residues forming the "strong" calcium binding site (Pro175, Val/Ala177 and Asp200) Ca1 are marked with dark green ball and those forming the weak calcium binding site Ca2 (Thr16 and Asp260) are marked with pale green ball. The Ca2 site is unique for proteinase K.

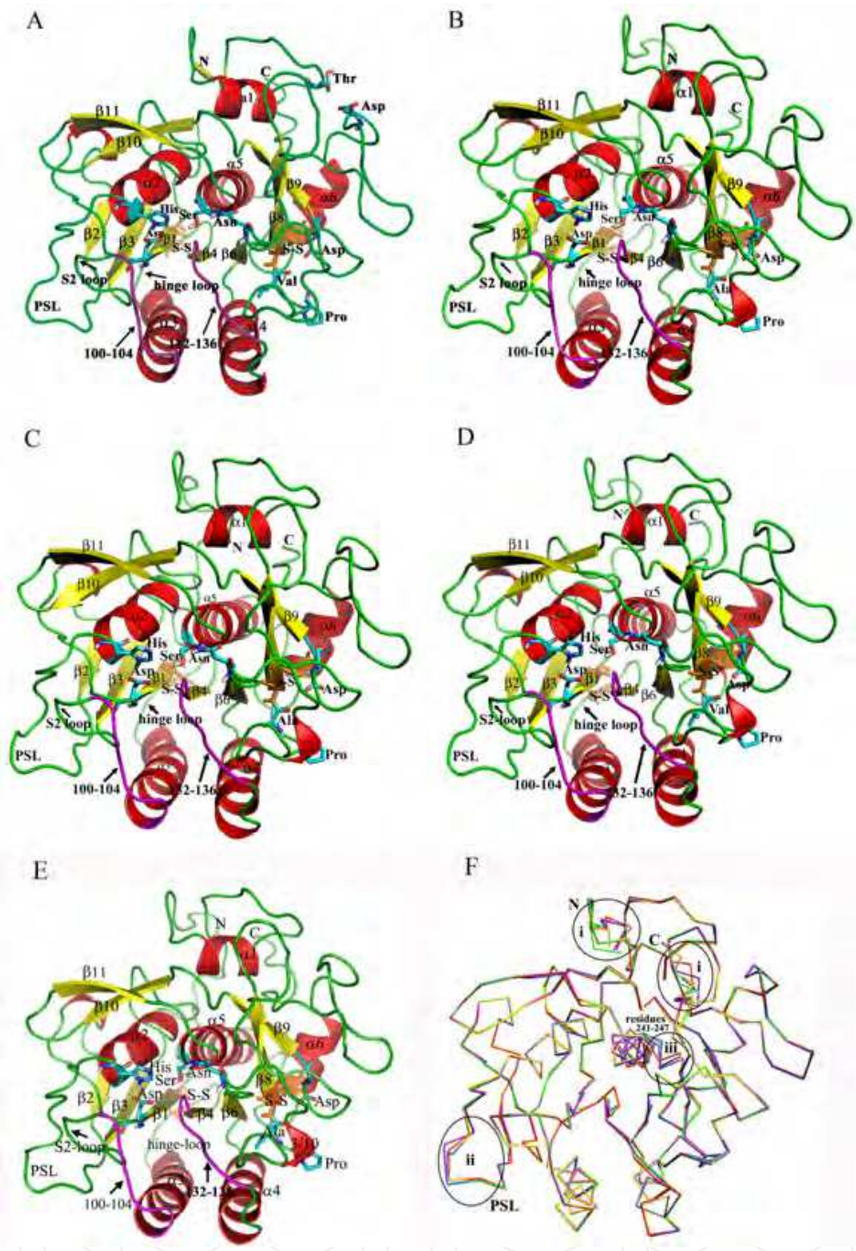

Fig. 4. Structural representations of the homology models of cuticle-degrading proteases. (A) 1IC6, (B) PR1, (C) VCP1, (D) Ver112, (E) PL646 and (F) backbone superposition of the four cuticle-degrading proteases and their template structure proteinase K with PDB code 1IC6. The α helices, β strands and loops are colored red, yellow and green, respectively. Substrate-binding segments 100-104 and 132-136 (1IC6 numbering) are in purple and disulfide bridges in orange. The residues of catalytic triad (Asp39, His69 and Ser224), oxyanion hole (Asn161), disulfide bridges (S-S), and calcium binding sites are rendered as stick models. In plot (F) the backbones of 1IC6, PR1, VCP1, Ver112 and PL646 are colored yellow, blue, green, red and purple; and the structural regions exhibiting relatively large conformational difference are labeled: (i) N- and C-Termini; (ii) surface-exposed polar loop (PSL) located between β2 and α2; and (iii) the loop region (residues 241-247) located between α5 and α6.

Quantitative comparisons between these structural models were performed by using least-square fitting method implemented in Swiss-Pdbviewer (Guex & Peitsch, 1997). The structure backbones were superimposed pairwise onto each other, achieving the backbone root mean deviation (RMSD) values with the range of 0.04-0.80 Å. The order of structural difference between these models is: PR1-VCP1 (0.04 Å) < PR1-PL646 (0.05 Å) < Ver112-PL646 (0.21 Å) < Ver112-PR1 (0.34 Å) = VCP1-PL646 (0.34) < VCP1-Ver112 (0.35 Å) < Ver112-1IC6 (0.58 Å) <1IC6-PR1 (0.75 Å) = 1IC6 -VCP1 (0.75 Å) < 1IC6-PL646 (0.80 Å), suggesting that the cuticle-degrading protease are more similar in structure to each other than to proteinase K. This is in agreement with the postulation that the higher the amino acid residue sequence identity between the proteins, the more similar the structures between them. The sequence identities of PR1-VCP1, PR1-PL646, Ver112-PL646, Ver112-PR1, VCP1-PL646, VCP1-Ver112, Ver112-1IC6, 1IC6-PR1, 1IC6 -VCP1 and 1IC6-PL646 are 78.6%, 74.6%, 71.1%, 69.5%, 68.0%, 64.3%, 64.1%, 66.4%, 62.5% and 62.0%, respectively.

In the crystal structure of proteinase K, four of the five cysteines form two disulfide bonds: Cys34-Cys123 and Cys178-Cys249, whereas Cys73 is free. Interestingly, all the four cuticle-degrading proteases contain the five positionally equivalent cysteines and the two corresponding disulfide bridges are also presented in the resultant structural models of the cuticle-degrading proteases. Close inspection of these models reveals that the free sulfur atom in Cys73 makes close contacts with the active site residues His69(O), Ser224(O), and Ser132(O_γ), for which the function consequence has yet to understand.

The catalytic triad residues Asp39, His69 and Ser224 and the component of the oxyanion hole residue Asn161 are completely conserved among the proteinase K and cuticle-degrading proteases as shown in the multiple sequence alignment plot (Figure 3), resulting in the perfectly structurally conserved architecture of the catalytic triad and oxyanion hole among the structural models of these enzymes (Figure 4). In proteinase K, two polypeptide segments of residues 100-104 and 132-136 constitute the two sides of the substrate-binding channel, where the P4, P3, P2 and P1 residues of the substrate are accommodated as the central strand to form a three-stranded antiparallel β sheet with residues in the S4, S3, S2 and S1 sites of the enzyme (Wolf et al., 1991). Among the four cuticle-degrading proteases, the residues equivalent to substrate-binding regions of proteinase K are well conserved with only subtle amino acid variations being found in the S1 and S4 substrate-binding pockets (Figure 3 and 5).

Despite the essentially global similarity between these structural models, relatively large conformational differences in local structures can still be found upon the superposition of these structural models (Figure 4F). Close inspection of Figure 4F reveals three regions exhibiting large backbone conformational differences: i) the N- and C-terminal regions, which exhibit the largest difference; ii) the surface-exposed loop comprising residues 59-68 with a high percentage of polar residues, and is thus termed polar surface loop (PSL); iii) the surface-exposed loop region (residues 241-247) located between α5 and α6. These large conformational differences are brought about by residue insertions or deletions within these regions as indicated by the sequence alignment (Figure 3). The most insertions or deletions of the target sequence relative to the template 1IC6 are found in the N- and C-termini, thus leading to the largest differences in conformation between these cuticle-degrading proteases. Other insertions are only observed in PSL and in loop region connecting α5 and α6, i.e, in PSL, PR1, VCP1 and PL646 have one residue insertion between positions 61 and 62 relative to the template sequence 1IC6; in loop 241-247 the cuticle-degrading enzymes PR1, VCP1 and PL646 have one insertion between positions 244 and 245. The few insertions or

deletions that are observed merely in loops, in conjunction with the high degree of sequence identity, can be used to explain the virtually identical structural models of these proteases. However, as will be described and discussed later, the subtle differences in architecture of the substrate-binding regions, which arise from variation in amino acid sequence, can be used to predict differences in function properties between these enzymes.

4.3 Factors contributing to the stability of molecular structures

4.3.1 Ca^{2+}-binding sites

Many proteases in the peptide S8 family contain one or more Ca^{2+}-binding sites and binding of calcium cations enhances the thermal stability of the proteases which in turn increase their resistance again proteolysis, either by itself or by other proteases (Bajorath et al., 1989; Betzel et al., 1988; Betzel et al., 1990; Müller et al., 1994). Two Ca^{2+} cations were found in the high resolution crystal structure of proteinase K (Figure 1 and 4A) (Betzel et al., 2001). The first Ca^{2+} is coordinated tightly by the $O_{\delta1}$ and $O_{\delta2}$ of Asp200 and the carbonyl oxygen atoms of Pro175 and Val177, and as such this site is termed strong Ca^{2+}-binding site Ca1. Intuitively, the Ca1 is able to stabilize the regions around itself, especially the long loops connecting β7 and β8 and β8 and β9. The second Ca^{2+} is a weakly bound Ca^{2+}, which is coordinated by Ca2 site consisting of the $O_{\delta1}$ and $O_{\delta1}$ of Asp260 and the carbonyl oxygen atom of Thr16. The Ca2 stabilizes to some extent the N- and C-terminal regions of the molecular structure. Among the four cuticle-degrading proteases, Ver112 and PL646 completely preserve the Ca1 site, whereas PR1 and VCP1 have residue substitution at position 177, i.e., an Ala in Pr1 and VCP1 substitutes for Val in 1IC6 (Figure 3). Although such substitution may have influence on the calcium affinity, we consider that such effect may be minor because the carbonyl oxygen of Ala177, coupled with carbonyl oxygen of Pro175 and carboxyl oxygens of Asp200, can still coordinate Ca^{2+} in a manner similar to that in 1IC6. In the case of the Ca2 site, the Thr16 in 1IC6 is replaced by an Arg in the four cuticle-degrading enzymes and the Asp260 in 1IC6 is replaced by a Val in PR1, Ver112 and PL646 and by Ala in VCP1, possibly leading to the loss of the ability of these cuticle-degrading enzymes to bind the second calcium cation due to the lack of carboxyl oxygens.

4.3.2 Disulfide bonds

It has been shown that disulfide bonds play an important role in the stability of some proteins by an entropic effect (Matsumura et al., 1989), usually the globular proteins secreted to extracellular medium (Sevier & Kaiser, 2002). As mentioned above, two disulfide bonds equivalent to those in proteinase K were also observed in the homology models of these four cuticle-degrading proteases (Figure 1, 3 and 4). The disulfide bridge Cys34-Cys123 connects the N-terminus of β1 at whose C-terminus lies the catalytic residue Asp39 and the loop (residues 118-126) connecting α3 and β4. Although this loop is located opposite the substrate-binding regions and is relatively far away from the catalytic triad, it links the α3 following the substrate-binding segment residues 100-104 and β4 preceding the other substrate-binding segment residues 132-136. Therefore, this loop can be considered as a "hinge" capable of modulating the orientation of the substrate-binding segments. As a result, the disulfide bond Cys34-Cys123 may participate in such modulation through contributing to the stability of this loop. On the other hand, this disulfide bond may also affect the dynamic behavior of the catalytic residue Asp39 via the rigid strand β1. The other disulfide bridge Cys178-Cys249 connects the N-terminus of β8 (located next to the S1

pocket) and α6, attaching the peripheral α6 to the main body of proteases, contributing to the stability of the C-terminal region. In addition, since β8 is located adjacent to the S1 substrate-binding pocket, Cys178-Cys249 may also influence the orientation of the S1 residues via a loop comprising residues 171-177.

4.3.3 Hydrogen bonds and salt bridges

Hydrogen bonds have been considered to contribute to the overall stability of the protein structure due to their large number and wide distribution (Shirley et al., 1992), whereas salt bridges contribute to a large extent to only the local stability because of its limited number and localized distribution (Arnorsdottir et al., 2005). The numbers of hydrogen bonds/salt bridges in structural models of proteinase K, PR1, VCP1, Ver112 and PL646 are 223/14, 189/12, 189/12, 195/13, and 199/8, respectively (Table 2). Here we mainly focused on the hydrogen bonds and salt bridges that serve to stabilize certain sites of interest. For example, a salt bridge network Arg12:Asp187:Lys/Arg18, which is found in all these four cuticle-degrading proteases, contributes to the stability of the N-terminal region of these proteases. This salt bridge network does not occur in proteinase K due to the lack of positively charged residue at position 18. However, the Ca2 cation, which does not exist in cuticle-degrading proteases, acts as an important factor to stabilize the N-terminus in proteinases K. Another bridge network, Arg52:Glu50:Lyr/Arg80, is found to be conserved throughout the five enzymes, connecting and stabilizing two surface loops between β1 and β2 (residues 40-52) and between α2 and β3 (residues 79-88). A completely conserved salt bridge, Asp117:Arg121, together with the disulfide bridge Cys34-Cys123, anchors and stabilizes the "hinge" loop containing residues 118-126. Additionally, two or more salt bridges are observed between two regions carrying multiple successive negatively or positively charged residues, i.e., Asp26-Glu/Asp27 and Lys86-Lys87, contributing to the stability of the long loop connecting α1 and β1 and of the relatively short loop between α2 and β3, although the stability effect is weaker in Ver112 and PL646 than in 1IC6, PR1 and VCP1 due to the reduction in the number of negatively charged residue in Ver112 and PL646 (replacement of Glu/Asp with Thr). There is a salt bridge, Asp112:Arg147, in the two proteases 1IC6 and Ver112 that is able to bridge α3 and α4, which are located adjacent to the two substrate-binding segments composed of residues 100-104 and 132-136. This salt bridge does not exist in PR1, VCP1 and PL646 due to the replacement of Arg147 with Ala, although the position 112 is occupied by the negatively charged residue (Asp or Glu) throughout the five proteases. In PR1 and VCP1, a salt bridge network, Lys250:Asp254:Lys251, is observed to contribute to the stability of the C-terminal helix α6, while only one salt bridge, Arg250:Asp254, is found in α6 of 1IC6, and no salt bridge in α6 of Ver112 and PL646. Interestingly, another structural factor capable of stabilizing α6, i.e., the disulfide bond Cys178-Cys249 is found in all these four cuticle-degrading proteases and proteinase K.

The region of residues 162-169 is located in the vicinity of S1 pocket and some of its residues form the bottom of the S1 pocket. For all these proteases except for PL646, at least one salt bridge or salt bridge network is found in this region contributing to the stability of this region. For example, 1IC6 contains a salt bridge, Asp165:Arg167, PR1 and Ver112 share a salt bridge, Asp162:Arg164, and VCP1 contains a salt bridge network, Asp162:Arg168:Asp165. Although PL646 contains no salt bridge in this region, a number of hydrogen bonds are observed in this region that can also stabilize the bottom of S1 pocket.

Taken together, the salt bridges coupled with the hydrogen bonds contribute to the stability of the S1 pocket bottom, which may facilitate the precise orientation of the P1 residue of the substrate for nucleophilic attack by the Ser.

Protease	RMSD[a] (Å)	SASA[b] (nm^2)	Rg[c] (nm)	NHB[d]	NNC[e]	NSB[f]	ENE[g]	DIH[h]	SSE[i]		
									α helix	β sheet	Turn
1IC6	0	109.2	1.67	223	134896	14	–9288.2	0	69	66	43
PR1	0.75	113.4	1.67	189	129252	12	–8560.3	0	67	66	42
VCP1	0.75	111.0	1.67	189	128896	12	–8560.0	0	70	64	47
Ver112	0.58	106.6	1.66	195	132572	13	–8732.7	1	70	66	43
PL646	0.80	111.7	1.69	199	130180	8	–8464.9	0	71	66	39

[a] Backbone RMSD with respect to 1IC6.
[b] Total solvent accessible surface area.
[c] Radius of gyration.
[d] Number of hydrogen bonds. A hydrogen bond is considered to exist when the donor-hydrogen-acceptor angle is larger than 120° and the donor-acceptor distance is smaller than 3.5 Å.
[e] Number of native contacts. A native contact is considered to exist if the distance between two atoms is less than 6 Å.
[f] Number of salt bridges. A salt bridge is considered to exist if the distance between two oppositely charged residues is within 6 Å.
[g] Potential energy after energy minimization in the GROMOS96 force field.
[h] Number of residues in the disallowed regions in the Ramachandran plot.
[i] Number of residues in the corresponding secondary structure elements.

Table 2. Geometrical properties of proteinase K crystal structure 1IC6 and structural models of the four cuticle-degrading enzymes PR1, VCP1, Ver112 and PL646.

Charged residue clusters are also found in two surface-exposed loops: the PSL (residues 59-68) and the loop composed of residues 94-101. PSL is located before the catalytic triad residue His69. The loop 95-101 is located in close proximity to the S2 pocket and partially participates in the formation of the S2 pocket, and therefore it is referred to as the S2-loop. A completely conserved salt bridge network Asp65:Lyr94:Asp97 is found in all these five proteases, bridging the PSL and the S2-loop together contributing to the stability of these two loops. Two additional salt bridge networks (Asp65:Lyr94:Asp98 and Arg64:Asp98:Lyr94) capable of enhancing the stability of these two loop are observed in 1IC6 and Ver112. The stability of the S2-loop is further enhanced by an absolutely conserved hydrogen bond network Asp97-[Gly100, S101] in these five proteases. Additionally, a salt bridge Glu43:Arg64, which is found only in proteinase K and Ver112 but not in other proteases, contributes to the stability of the PSL. Another important factor contributing to the stability of the PSL is the hydrogen bond and hydrogen bonding network, i.e., a completely conserved hydrogen bonding network Asp65-[Gly68, Thr71] is observed in all these five enzymes; and the number of hydrogen bonds involved in stabilizing the PSL is 10, 9, 7, 8 and 8 in 1IC6, PR1, VCP1, Ver112 and PL646, respectively. Taken together, we can conclude that a relatively large number of hydrogen bonds in conjunction with a relatively small number of salt bridges constitutes the stability determinants of the PSL. Because of its long loop length, close proximity to activity center and solvent-exposed character, the

stability of the PSL loop is important for the global structural stability or even for the catalytic activity of these proteases. This is reflected by the fact that the calcium cation is observed to stabilize PSL in two members of proteinase K subfamily, the VPRK from *Vibrio* sp. PA44 (PDB code 1SH7) (Arnorsdottir et al., 2005) and the thermitase from *Thermoactinomyces vulgaris* (PDB code 1THM) (Teplyakov et al., 1990).

4.3.4 Aromatic ring stacks

The aromatic ring stacking interaction between aromatic residues can aid in enhancing the structural stability of the protein (Siezen et al., 1991). Two absolutely conserved aromatic ring stacking interactions are found in residue pairs Tyr23-Tyr25 and Tyr/Phe59-Phe/Tyr113. The former contributes to the stability of the N-terminal region; the latter makes contribution to the stability of the PSL and α3. A conserved aromatic ring stacking interaction is observed between residue pair Tyr36-Phe/Tyr91 in 1IC6, PR1, Ver112 and PL646, contributing to the stability of both β1 and β3. Such an aromatic stacking interaction does not exist in VCP1 due to the replacement of the aromatic residue (Phe or Tyr) at position 91 by Leu.

4.4 Substrate-binding region and electrostatic surface potential

4.4.1 Substrate-binding sites/pockets

The substrate-binding region in subtilisin proteases is generally described as a surface channel or crevice that is able to accommodate at least six amino acid residues (P4-P2′) within the substrate such as a polypeptide chain or a pseudo-substrate (i.e., the inhibitor) (Siezen & Leunissen, 1997). In the crystal structure of proteinase K in complex with the inhibitor methoxysuccinyl-Ala-Ala-Pro-Ala-chloromethyl ketone (PDB code 3PRK) (Betzel et al., 1993; Wolf et al., 1991), the P4-P1 residues of the substrate slot in between two extended protease segments of residues 100-104 and 132-136, leading to the formation of a three-stranded antiparallel β sheet (Wolf et al., 1991). The leaving segment P1′-P2′ of the substrate runs along the protease segment of residues 220-222, exhibiting a weak binding to the enzyme. According to the crystal structures of 3PRK and 1IC6, the substrate-binding sites of the cuticle-degrading enzymes are identified (Figure 3 and 5). The S2′ site is a hydrophobic pocket formed primarily by residues 192, 221 and 222. The S1 is a distinct, large and elongated pocket that is primarily formed at the side by residues 132-135 and at the bottom by residues 158-161. This pocket is also surrounded at the rim by residue 162, at the bottom end by residue 169, and at the top by a segment of residues 222-225 at which the nucleophilic residue Ser224 is located. Compared to S1 pocket, the S2 site is a less distinct and relatively smaller pocket, which is bounded at one side by residue 100 and at the other side by the catalytic triad residue His69, at the bottom by the hydrophobic residue Leu96 and the catalytic triad residue Asp39, at the bottom end by residue 40, and at the rim by residue 67, respectively. S3 site is formed by only one residue at position 101, which is not a pocket because the side chain of Ser101 is located at the exterior of the substrate-binding region, forming a convex surface at this site (Figure 5). The residue 100 may also have the potential to interact with the P3 side chain due to their close proximity observed in the proteinase K-inhibitor complex structure. S4 site is located between two segments of residues 100-104 and 132-136, forming a very distinct and large pocket. This pocket can be divided into two subsites, S4a and S4b. S4a is formed by residues 96 and 107 at the bottom, residue 133 at the side, and residue 102 at the rim, respectively. S4b consists of residue 104 at

the side, residue 141 at the bottom, and residues 135-136 at the rim, respectively. It is important to point out that the sizes of the substrate residue-binding pockets are determined by side chains of the pocket-forming residues.

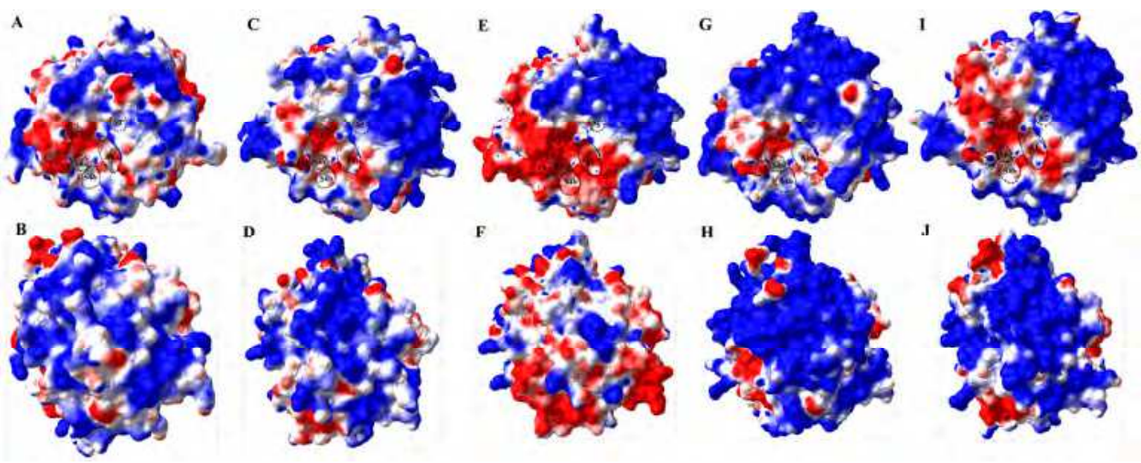

Fig. 5. Electrostatic surface potentials of (A, B) 1IC6, (C, D) PR1, (E, F) VCP1, (G, H) Ver112 and (I, J) PL646. Plots on the top/bottom are the front/back surface of the electrostatic potentials of these proteases, respectively. The positively and negatively charged electrostatic surfaces are colored blue and red, respectively. The approximate locations of the substrate-binding sites and/or pockets, S2′, S1, S2, S3, S4a and S4b are indicated.

We note that the amino acid residues forming the substrate-binding sites S2′ and S3 are completely conserved throughout the proteinase K and the four cuticle-degrading proteases investigated here, while those forming the pockets S1, S2 and S4 are observed to be variable. For example, variable residues within the S1 pocket are found at positions 162 and 169, which, as described above, are residues located at the rim and bottom end of this pocket, respectively. In the four cuticle-degrading proteases, the acidic residue Asp162 substitutes for the neutral Asn162 in the proteinase K. Despite their common side chain conformation, the acidic residue Asp162 make the S1 pocket carry more electro-negative characteristics (Figure 5), which in turn may shift the substrate specificity to the positively charged P1 residues (Siezen et al., 1991; Siezen & Leunissen, 1997). In addition, it has been observed that the electro-negative character can increase flexibility of a protease (Pasternak et al., 1999), especially the flexibility of the active site region (Kumar & Nussinov, 2004). We therefore assume that the Asp162 in the cuticle-degrading enzymes should increase the flexibility of the S1 site, which in turn may enhance the catalytic efficiency of the cuticle-degrading proteases and subsequently the infection virulence by the fungi. Position 169 is occupied by the Tyr in 1IC6, VCP1 and PL646 and by the Thr in PR1 and Ver112. It should be noted that the P1 specificity of subtilisin BPN′ can be significantly affected by residue replacements at this position using site-directed mutagenesis technique (Estell et al., 1986; Wells et al., 1987). Most of the residues within the S2 pocket are conserved throughout the five proteases except for the one at position 67, which is occupied by Asn in 1IC6 and PL646 but by the His in PR1, VCP1 and Ver112, implying a slight preference of the latter three cuticle-degrading proteases at the low pH for the negatively charged P2 residues. The largest number of variable residues in the substrate-binding region is found within the S4 pocket, i.e., there are five positions, 103, 104, 107, 136 and 141, that are occupied by different residues among

these five proteases. For example, Gln103 in proteinase K is replaced with Ser103 in the four cuticle-degrading enzymes, enlarging the S4 pocket of cuticle-degrading proteases due to relatively smaller side chain of Ser than that of the Gln. The Tyr104 in PR1, VCP1, 1IC6 and PL646 is replaced by a Leu in Ver112. Because Tyr104 has been shown to act as a flexible lid to the S4 pocket in the structures of subtilases (Siezen et al., 1991; Siezen & Leunissen, 1997), the Leu104 at the equivalent location broadens the entrance for P4 residues and simultaneously increases the hydrophobic character of the S4 pocket. Two amino acid residue variations, i.e., the substitution of a Val in VCP1 for Ile107 in 1IC6, PR1, Ver112 and PL646, and the substitution of a Leu in Ver112 for Val141 in 1IC6, PR1, VCP1 and PL646, likely have a minor influence on the size and hydrophobic character of the S4 pocket because Ile/Val107 and Val/Leu141 are buried to a large extent within the bottom of S4 pocket and all have strong hydrophobic character. The presence of Pro136 in VCP1 leads to a larger rim of the S4 pocket because of its larger size compared to the equivalent Gly136 presented in 1IC6, PR1, Ver112 and PL646. Interestingly, the amino acid residues at positions 136 and 104 can be seen as two gates for the entrance of the S4 pocket, and as such the presence of larger Pro may affect entry of the P4 residues into the S4 pocket. The hydropathy score of the S4 pocket was calculated approximately as the sum of the hydropathy value (Kyte & Doolittle, 1982) for all the residues within the S4 pocket, yielding values of 13.8, 13.8, 13.5, 18.5 and 13.8 for 1IC6, PR1, VCP1, Ver112 and PL646, respectively, indicating that the S4 pockets of these proteases have strong and comparable hydrophobic character, with the strongest hydrophobicity observed in Ver112.

4.4.2 Electrostatic surface potential

The electrostatic surface potentials of these five proteases were calculated using Poisson-Boltzmann method with Swiss-PdbViewer and the results were shown in Figure 5. Many electrostatic potential features are common to the surfaces of these proteases, i.e., the back surfaces of these proteases are dominated by electro-positive potential except for that of VCP1 (Figure 5F), which exhibits the mixed distribution of positively (blue color) and negatively (red color) charged potentials; the front surfaces of these enzymes exhibit a dual feature of both positively and negatively charged potentials, although the majority of the front surfaces are positively charged. Close inspection of the front surfaces reveals that the electro-negative potentials are mainly concentrated in and/or around the substrate-binding regions of these enzymes, especially those of VCP1 and PL646 (Figure 5E and I). For the other proteases, sporadic distribution of the electro-negative spots can be found outside the substrate-binding sites. The functional significance of the electrostatic surface potential distribution will be discussed in the "Functional implication" section.

4.5 Functional implication

It has been shown that the high-accuracy homology models can be obtained if the sequence identity between the target and template is greater than 50%, with the accuracy of the modeled structures being comparable to that of the medium-resolution NMR or X-ray structures (Baker & Sali, 2001). The high degree of sequence identity of these four cuticle-degrading proteases to the template proteinase K suggests that our structural models are very accurate, as confirmed by comparison of homology models with the X-ray crystallographic structures that we determined later (Liang et al., 2010), which exhibits that for the Ver112 and PL646, the backbone RMSD between the theoretically modeled and experimentally determined structures is 0.57 and 0.64 Å, respectively. Such highly accurate

structural models guarantee the accuracy of prediction for Ca^{2+}-binding site, disulfide bridge, hydrogen bond, salt bridge and aromatic ring stack that contribute to the global or local stability of the enzyme structures, and can also be used to investigate differences in functional properties such as substrate specificity and catalytic activity among these proteases.

As mentioned above, although the four cuticle-degrading enzymes were predicted to contain no weak Ca^{2+} cation Ca2 present in 1IC6, several hydrogen bonds and salt bridge networks were observed within or close to the Ca2-equivalent site to act as stabilizing factors for the N- and C-terminal regions of the cuticle-degrading enzymes (for details see (S.Q. Liu et al., 2007b)). This may explain why the presence of EDTA has a minor effect on the activity of proteinase K and cuticle-degrading proteases (S. Q. Liu et al., 2011; Müller et al., 1994; J.K. Yang et al., 2005b). Of interest is that another Ca^{2+} found in the vicinity of the PSL of proteinase K-like serine protease structures with PDB codes 1SH7 (Arnorsdottir et al., 2005) and 1THM (Teplyakov et al., 1990) does not exist at the equivalent location in the cuticle-degrading proteases investigated here. The abundant hydrogen bonds and salt bridges observed in PSL can contribute to its stability in these proteases.

Our comparative modeling study, together with structural studies using X-ray crystallographic and NMR techniques, indicates that members of the S8 peptidase family have an overall highly rigid globular fold (Betzel et al., 2001; Liang et al., 2010; S. Q. Liu et al., 2010, 2011; Müller et al., 1994; Martin et al., 1997; Siezen et al., 1991; Siezen & Leunissen, 1997). The globular fold can be considered as the consequence of combination of various protein-folding driving forces, including the hydrophobic force that maximizes the entropy of the protein-solvent system through minimizing the solvent-accessible surface area of the protein, making the overall protein shape spherical; and enthalpic contribution through favorable energetic contacts such as van der Waals contacts, electrostatic and hydrogen bonding interactions. It has been proposed that the compact globular packing and high rigidity of the proteinase K-like serine proteases have evolved as the protective measures against autolysis (S. Q. Liu et al., 2010, 2011; Martin et al., 1997). However, a certain degree of flexibility within the substrate-binding regions is required to allow recognition and binding of the substrates with high affinity (Lange et al., 2008; S. Q. Liu et al., 2010, 2011; Perica & Chothia, 2010; Tao et al., 2010). For the substrate-binding regions, the delicate balance between the rigidity and flexibility may play important roles in maintaining structural stability and modulating substrate binding specificity and affinity. The important factors involved in determining rigidity and flexibility of local structural region are hydrogen bonds and salt bridges, especially their number and distribution. An example of crystallographic study on a proteinase K-like protease, SPRK from the psychrotroph *Serratia* species (PDB code 2B6N) shows that a strong hydrogen bond network, Asn97-[S99, S101] brings its S2-loop into a 'hub and spokes' arrangement with high rigidity, which may explain the relatively low binding affinity (higher K_m value) of SPRK towards the synthetic substrate suc-Ala-Ala-Pro-Phe-nitroanilide (Helland et al., 2006). In addition, the tight S2-loop may also influence the substrate specificity profile of SPRK (Helland et al., 2006) because of the conformational selection (Monod et al., 1965; Tobi & Bahar, 2005) and/or induced fit (Koshland, 1958) mechanisms of substrate binding. In the case of the cuticle-degrading proteases studied here, a conserved hydrogen bonding network, Asp97-[Gly100, S101], and a conserved salt bridge network, Asp65:Lyr94:Asp97, are observed to contribute to the stability of the S2-loops. However, for PR1, VCP1, Ver112 and PL646, their number of hydrogen bonds/salt bridges involved in stabilizing the S2-loop is 4/1, 4/1, 5/3 and 7/2,

respectively, implying more rigid S2-loop in Ver112 and PL646 than in the other two enzymes. This leads to the speculation that Ver112 and PL646 may have relatively lower P2 affinity compared to Pr1 and VCP1.

The variation in substrate specificity of subtilisin is most likely to be caused by variable residues within the substrate-binding sites, especially by those whose side chains interact directly with the P1 and P4 residues of the substrate (Siezen et al., 1991; Siezen & Leunissen, 1997). We therefore make some prediction of the variation in substrate specificity among the cuticle-degrading proteases according to this principle. As mentioned above, the Asp162 substitution in the four cuticle-degrading enzymes for Asn in proteinase K could not only enhance the catalytic efficiency but also increase the specificity to the basic P1 residues. The residue 169 is located at the bottom end of the S1 pocket and is either Tyr in proteinase K, VCP1 and PL646 or Thr in PR1 and Ver112. Inspection of the structural models reveals that the bottoms of the S1 pocket of these five proteases remain the same width because the side chains of both Tyr and Thr rotate away from the S1 pocket bottom end (Figure 5), in agreement with the docking data showing that Tyr in 1IC6 does not interact directly with the P1 residue of a substrate (Helland et al., 2006). We therefore consider that this observed residue variation at position 169 may have a minor effect on substrate specificity of these cuticle-degrading enzymes. Five positions with variable residues are found within S4 pocket suggesting that these proteases have most variable specificity for the P4 residues of substrates. For example, the replacement of Gln103 in proteinase K with a Ser in all these four cuticle-degrading proteases increases not only the size but also the hydrophobicity of the S4 pocket to a certain extent, thus broadening the specificity profile of the P4 substrate residues. In Ver112, the Leu substitution at position 104 for Tyr in the other proteases leads to the increased preference of Ver112 for large and hydrophobic P4 residues in comparison with the other proteases. VCP1 may have a preference for relatively small P4 residues compared to the other proteases due to its Pro substitution for Gly at position 136, which narrows the entrance to the S4 pocket. Note that the predicted changes in substrate specificity of these cuticle-degrading proteases based on the structural models need to be verified by experimentally determining the kinetic data of the enzyme-substrate interaction, and this will be further discussed later in this chapter.

The most pronounced feature of the electrostatic surface potential of these cuticle-degrading proteases is that their substrate-binding regions are commonly negatively charged whereas a large fraction of the other surfaces is positively charged. As mentioned above, the anionic feature of the substrate-binding regions is able to increase the local conformational flexibility of these regions, which in turn could increase the substrate affinity and catalytic efficiency. It has been shown that the cuticles of many nematodes and insects contain abundant acidic residues and as such are heavily negatively charged under neutral condition (Bidochka & Khachatourians, 1994; Blaxter et al., 1992; Cox et al., 1981; Himmelhoch & Zuckerman, 1978; Murrell et al., 1983). Therefore, the dominated electro-positive surface outside the substrate-binding regions will facilitate the diffusion and adsorption of the cuticle-degrading proteases to their substrate - the cuticle of nematodes or insects - due to the electrostatic attraction between oppositely charged molecules, thus leading to efficient degradation of cuticle by enzymes. In addition, the large fraction of the positively charged surfaces can also explain why the cuticle-degrading proteases secreted by nematode-parasitic fungi studied here are all alkaline proteases.

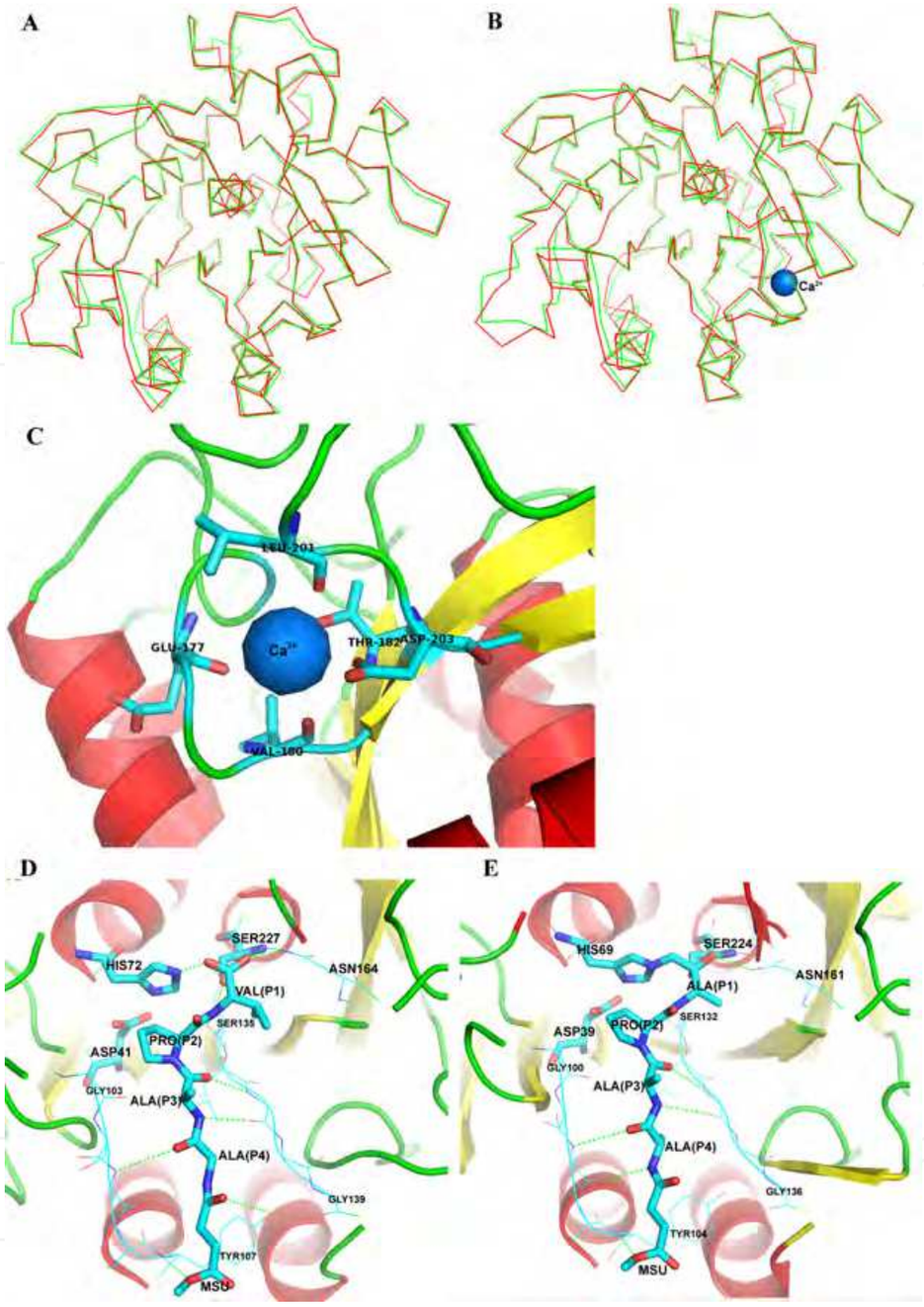

Fig. 6. Crystal structures of Ver112 and PL646 and their comparison with corresponding homology models. (A, B) Backbone superposition of crystal structure and homology model of Ver112 (A) and PL646 (B). Experimental and theoretical structures are shown in red and green, respectively; and calcium cation in PL646 is shown as a blue ball. (C) Residues coordinating with Ca^{2+} (Ca1 site) in PL646. (D, E) Substrate-binding site of PL646 in complex with the inhibitor MSU-AAPV-ketone (D) and of proteinase K in complex with the MSU-AAPA-ketone (E). Residues of the substrate-binding site, catalytic triad, oxyanion hole and substrate P4-P1 are labeled; the carbon, nitrogen and oxygen are shown in cyan, blue and red, respectively; the hydrogen bonds between the substrate and enzyme are denoted by dashed green lines.

5. Crystal structures of two cuticle-degrading proteases and their kinetic data

In order further to investigate the structure-function relationship of the cuticle-degrading proteases and verify the predicting results of some structural and functional properties based on the above modeled homology structures, we select two of the above proteases, Ver112 and PL646, for crystallographic and kinetic studies (Liang et al., 2010).

5.1 Comparison between the crystal structures and homology models

The structures of two cuticle-degrading proteases, Ver112 and PL 646, were solved with X-ray crystallographic method to resolutions of 1.65 Å and 2.1 Å, respectively, which were deposited in the PDB structure database with accession codes of 3F7M for Ver112 and 3F7O for PL646. As expected, structural comparison reveals that the structures of the experimentally determined and theoretically modeled proteases are nearly identical (Figure 6A and B), giving the backbone RMSD values of 0.57 Å (Ver112) and 0.64 Å (PL646), respectively. Consequently, the secondary structural element components, architecture of the catalytic triad, and location of substrate-binding sites observed in the crystal structures are almost the same as those observed in the homology models. Two predicted disulfide bonds, Cys34-Cys123 and Cys178-Cys249 (proteinase K numbering), are also presented in the crystal structures of Ver112 and PL646. One Ca^{2+} cation is found in the crystal structure of PL646, which is coordinated with high affinity by carbonyl oxygens of Glu177, Val180 and Leu201, $O_{\gamma 1}$ of Thr182, and $O_{\delta 2}$ Asp203 (PL646 numbering, Figure 6C), forming a more precise Ca1 site than what is predicted based on the homology model. The weak calcium cation Ca2 present in proteinase K structure with PDB code 1IC6 is not observed in the crystal structure of PL646, in agreement with the prediction based on the homology model. In the case of Ver112, although the amino acid residues forming the Ca1 site are identical to those in PL646 and 1IC6, no Ca^{2+} was observed to bind to this site in the crystal structure. The possible reason for this is that Ver112 was crystallized in a Ca^{2+}-free buffer. Taken together, although the calcium cation has been considered as an important factor in enhancing the thermostability of serine proteases (Bajorath et al., 1989; Betzel et al., 1990; Müller et al., 1994; Siezen et al., 1991), the binding of such cation may not be indispensable for the structural stability, either globally or locally, because the presence or absence of the Ca^{2+} at the same site in different proteases does not affect the overall folding and local architecture of the enzyme structures, and other structural factors like the abundant van der Waals contacts, hydrogen bonds and salt bridges play a dominant role in maintaining the stability of protein structure. However, our molecular dynamics study on proteinase K shows that Ca^{2+} can have an effect on the functional properties of this protease through altering the rigidity/flexibility of the structural regions around the calcium cation (S. Q. Liu et al., 2011), suggesting that the difference in local dynamics can be related to functional difference between members of the same family.

Superposition of the structure of the protease PL646 in complex with the inhibitor MSU-AAPV-ketone (Figure 6D) with that of the proteinase K complexed with MSU-AAPA-ketone (PDB code 3PRK (Wolf et al., 1991); Figure 6E) gives a backbone RMSD of 0.69 Å. In both complex structures, the inhibitor MSU-AAPA-ketone lies well in the substrate channel located between the segments of residues 100-104 (residues 103-107 in PL646) and 132-136 (residues 135-139 in PL646); and the conserved backbone hydrogen bonding interaction between the substrate and the protein residues are also observed, indicating that the predicted substrate-binding pockets shown in Figure 5 are correct. Also, the

electrostatic surface potentials of the two crystal structures were also calculated and compared with those of their corresponding homology models, exhibiting the completely identical electrostatic potential distribution across the molecular surfaces (data not shown).

In the case of the substrate pockets, we have predicted above that the Tyr/Thr alteration at position 169 may not affect the size of the S1 pocket bottom because the side chains of both Tyr and Thr rotate away from the S1 pocket bottom end. In the crystal structure of Ver112, the Thr side chain adopts a similar orientation to that seen in the structural model; and in the crystal structure of PL646 in complex with substrate analogue MSU-AAPV-ketone, the Tyr side chain also rotates away from the S1 pocket bottom end and does not make contact with the P1 residue of a substrate, confirming our prediction and suggesting that residue variation at position 169 unlikely affects the substrate specificity. Further comparison between the crystal structures of Ver112 and PL646 shows that the Ver112 has a wider S4 pocket entrance than PL646 because the position 104 is occupied by residue Leu in Ver112 with smaller side chain compared to that of Tyr in PL646. The bottom of S4 pocket appears flatter and wider in Ver112 than in PL646, which is caused by residue difference at position 141, i.e., Leu/Val in Ver112/PL646, respectively. The relatively larger Leu side chain lies across the bottom of Ver112 S4 pocket, making it flatter and wider than that of PL646.

5.2 Kinetics analysis of Ver112, PL646, and proteinase K

In order to verify the predicted difference in substrate specificity and catalytic activity among cuticle-degrading proteases, the enzyme kinetic parameters of Ver112, PL646 and proteinase K towards several synthesized substrates were determined using a method as described in (DelMar et al., 1979). The polypeptide substrates were designed based on the sequence of the classical protease K inhibitor N-succinyl-Ala-Ala-Pro-Phe-p-nitroanilide (Suc-AAPF-pNA) through altering individual residues, achieving Suc-AAPD-pNA, Suc-NAPF-pNA and Suc-PAPF-pNA. The resultant kinetic data are listed in Table 3 (Liang et al., 2010). The lowest K_m value of 0.093 mM is observed to occur for proteinase K towards the substrate AAPD, exhibiting the strongest proteinase K-AAPD affinity. Cuticle-degrading protease PL646 shows approximately two orders of magnitude weaker affinity towards AAPD (1.21 mM) than proteinase K does (0.093 mM); and Ver112 may not bind AAPD as its K_m can not be determined. It seems likely that it is the electrostatic repulsion between Asp162 in S1 pocket and P1 residue of AAPD that reduces (in PL646) or abolishes (in Ver112) AAPD binding. The kinetic parameters of proteinase K towards NAPF can not be determined, possibly due to the relatively small S4 pocket of proteinase K in comparison to that of Ver112 and PL646. On the contrary, Ver112 and PL646 show both high affinity towards the substrates NAPF and PAPF, reflecting their capability of accommodating peptide substrates with large P1 and P4 residues. Furthermore, Ver112 binds with four-fold/two-fold higher affinity than does PL646 to NAPF/PAPF, respectively. This can be attributed to a wider entrance of S4 pocket in Ver112 than in PL646, allowing highly efficient entry of large P4 residues into S4 pocket of Ver112. PL646 has a relatively smaller S4 pocket than Ver112, possibly making it difficult to adopt appropriate arrangement to interact with P4 Ala of AAPF and AAPD, thus leading to the observed relatively weaker affinity of PL646 towards these two substrates compared to Ver112.

Proteases	AAPF		AAPD		NAPF		PAPF	
	K_m (mM)	K_{cat}/K_m ($s^{-1}mM^{-1}$)	K_m (mM)	K_{cat}/K_m ($s^{-1}mM^{-1}$)	K_m (mM)	K_{cat}/K_m ($s^{-1}mM^{-1}$)	K_m (mM)	K_{cat}/K_m ($s^{-1}mM^{-1}$)
Ver112	0.145	27354	N/A[a]	N/A[a]	0.164	2067	0.226	5206
PL646	1.42	17957	1.21	166	0.695	453	0.472	1576
PRK	0.31	33142	0.093	1229	N/A[a]	N/A[a]	0.111	3558

[a] Not available, meaning that the kinetics parameters can not be determined.

Table 3. Enzyme kinetic data of Ver112, PL646 and proteinase K towards several synthesized substrates. This table is modified from (Liang et al., 2010).

In the case of PL646, its lowest substrate affinity is observed towards AAPF (K_m = 1.42 mM) among the four synthesized substrates. However, this effect is offset by the highest turnover rate (170 1/s) resulting in the highest catalytic efficiency (K_{cat}/K_m) towards AAPF, which is one or two orders of magnitude larger than that towards PAPF, AAPD and NAPF (Table 3). Similarly, Ver112 and proteinase K also have the highest turnover rate towards AAPF, regardless of their high or low affinity towards this substrate, thus leading to the highest catalytic efficiency to the AAPF, explaining why the AAPF has always been used as the canonical substrate for enzyme activity assay. The relatively lower turnover rates of these three proteases towards AAPD, NAPF and PAPF may be caused by the stereochemical clashes while interacting with the large P1 (such as Asp in AAPD) and P4 (such as Pro and Asn in PAPF and NAPF). Out of these three newly designed substrates the PAPF can be considered as the best one for all the three proteases investigated here because of its observed high affinity and turnover rate. Our data show that, like the canonical serine protease proteinase K, the cuticle-degrading proteases also exhibit broad substrate specificity with preference for bulky hydrophobic or aromatic residues at the P1 and P4 positions of the substrate. The intrinsic reason for this is that both the substrate pockets S1 and S4 are large and hydrophobic. Interestingly, for PL646, although its S4 pocket is large to accommodate both large and small P4 substrate residues, its affinities towards AAPF (1.42 mM) and AAPD (1.21 mM) are weaker than those towards NAPF (0.695 mM) and PAPF (0.472 mM). We speculate that the large P4 residues (such as Asn in NAPF and Pro in PAPF) can form more non-bonding contacts, i.e., hydrogen bonding, hydrophobic and van der Waals contacts with S4 pocket than do the small residues (such as Ala in AAPF and AAPD), leading to a tighter association of protease with large residue than with small residue.

6. Dynamic behavior of proteinase K

A complete understanding of the structure-function relationship of a protein requires analysis of its dynamic behavior in addition to the static structure. Even for proteins with highly rigid structure (such as members within the S8 peptidase family), their dynamic behavior and molecular motions are still very important for understanding their function properties. The catalytic reaction of any enzyme is a dynamic process that occurs through a series of dynamic steps such as substrate binding, orientation, catalysis and product release. Detailed information on these dynamic steps as well as on how they are connected and regulated is necessary for a complete understanding of the enzymatic function. Therefore, we selected the classical serine protease proteinase K to investigate deeply into its dynamics using the molecular dynamics (MD) simulation technique (S. Q. Liu et al., 2010, 2011; Tao et

al., 2010). Because of the high degree of sequence and structure similarity between proteinase K and cuticle-degrading proteases, these proteases should also have similar or even identical dynamic features, which can be used to explain experimental data or be linked to functional properties of these enzymes. The content in this section would greatly facilitate the understanding of the structure-function relationship of this class of proteases.

6.1 Rigidity and flexibility of proteinase K and their functional implication

The crystal structure of proteinase K with PDB code 1IC6 (Betzel et al., 2001) was used as a starting model for the MD simulation. The GROMACS molecular dynamics package (Feenstra et al., 1999; Lindahl et al., 2001) was used with the GROMOS96 43a1 force field. The detailed molecular dynamics setup was described in (S. Q. Liu et al., 2010; Tao et al., 2010). The length of the MD simulation is determined by monitoring the convergence of RMSD relative to the starting structure during simulation. The conventional geometrical properties along the MD trajectory such as the number of hydrogen bonds (NHB), number of native contacts (NNC), number of residues in the secondary structure elements (SSE), radius of gyration (Rg), solvent accessible surface area (SASA) and RMSD were calculated using the programs g_hbond, g_mindist, do_dssp (Kabsch & Sander, 1983), g_gyrate, g_sas and g_rms within the GROMACS software package, respectively.

Analyses of the geometrical properties during simulation indicate that the structure of the proteinase K is stable with geometrical properties of NHB, NNC, Rg, SASA and RMSD fluctuating around their respective equilibrium values, and the well-defined global fold maintains well during simulation (data not shown and for details, see (S. Q. Liu et al., 2010)). Furthermore, the calculation of B-factors during simulation shows that proteinase K has a rigid structural core and a limited number of surface loops and links that show high structural flexibility. Among these flexible loops are those regions that participate in the formation of the substrate-binding site (such as segments containing residues 100-104, 132-136 and 160-169) and regions located near or opposite the substrate-binding site (such as segments of residues 59-68, 119-126 and 240-246). The presence of flexibility in the substrate-binding region, which has emerged from studies of many enzymes, supports either the induced-fit (Koshland, 1958) or conformational selection (Monod et al., 1965; Tobi & Bahar, 2005) mechanisms of substrate binding. In the induced-fit mechanism, a certain degree of flexibility should exist in the substrate-binding region for conformational adjustment induced by substrate binding. Under the conformation selection model, the high flexibility of the structure-binding region allows it to exist in an ensemble of conformational substates, one of which can be selectively bound by substrate, lowering the entropy barrier and biasing the equilibrium towards the complex conformation. We consider that these two mechanisms of substrate binding are not two independent and exclusive processes but rather they play a joint role in substrate recognition and binding due to the common prerequisite of conformational flexibility, which are important for both large-scale backbone concerted movement in the conformational selection and side chain adjustment/rotation in the induced-fit process. Accordingly, we believe that it is the high flexibility observed in the substrate-binding region that allows not only for the existence of conformational diversity but also the easy conversion between substates of this region, thus not only facilitating the efficient recognition and binding of substrates but also allowing interactions with different substrates with a variety of sequence and structure motif, broadening the substrate specificity of proteinase K. However, because of the overall structural rigidity of proteinase K, it seems that only the functionally essential flexibility is presented in certain local regions.

Taken together, it can be considered that the serine proteinase family has evolved to be as rigid as possible to resist autolysis or proteolysis by other proteases while remaining as flexible as necessary within certain structural regions to guarantee functional activity.

6.2 Flexibility of the catalytic triad

In order to investigate the dynamic nature of the catalytic triad, we also focus on the interaction strength between Asp39 and His69 and between His69 and Ser224 through calculating the interaction energies. The results show that a stronger electrostatic interaction occurs between His69 and Asp39 (Figure 7B) than between His69 and Ser224 (Figure 7C), resulting in a more stable and tighter association of Asp39-His69 than His69-Ser224 (Figure 7A). This implies that the proton transfer between His69 and Asp39 should be easier and more efficient than that between His69 and Ser224, leading to the speculation that the proton transfer from the $N_{\delta 1}$ of His69 to the carboxyl group of Asp39 may be the prerequisite for the proton transfer from the Ser224 O_{γ} to the His69 $N_{\varepsilon 2}$ (S. Q. Liu et al., 2010). An *ab initio* molecular orbital calculation of the catalytic triad (Nishihira & Tachikawa, 1996) showing a higher hydrogen transfer energy between the serine hydroxyl and the $N_{\varepsilon 2}$ of histidines imidazole than between the $N_{\delta 1}$ of histidine imidazole and carboxyl group of aspartate supports this speculation. In addition, the appropriate orientation of imidazole group within the catalytic triad can be obtained through the strong interaction between His69 and Asp39. Upon orientation, aspartate carboxyl abstracts a proton from the $N_{\delta 1}$ of imidazole group, resulting in an increase in pK_a and alkalinity of the imidazole group (Moult et al., 1985), which in turn is favorable for extraction of proton from the serine hydroxyl. As the consequence of weaker interaction of His69 with Ser224, Ser224 exhibits a higher degree of conformational freedom compared to Asp39 and His69, as indicated by B-

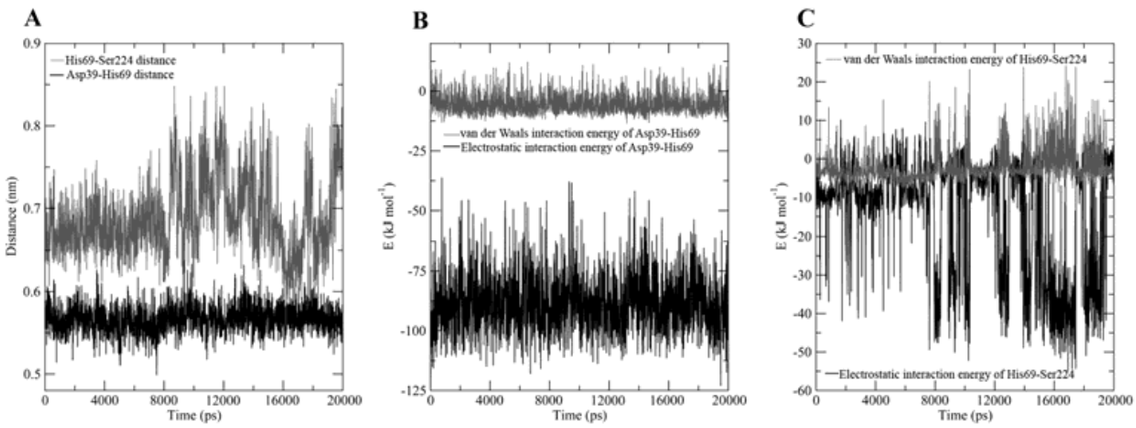

Fig. 7. Distances and interaction energies between residues within the catalytic triad during the molecular dynamics simulation. (A) The distances between the centers of mass of Asp39 and His69 (black line) and between centers of mass of His69 and Ser224 (grey line) as a function of simulation time. (B) The interaction energies between Asp39 and His69 as a function of time. The coulomb's electrostatic and van der Waals interaction energies of Asp39-His69 are shown in black and grey lines, respectively. (C) The interaction energies of His69-Ser224 as a function of time. The coulomb's electrostatic and van der Waals interaction energies of His69-Ser224 are shown in black and grey lines, respectively. This figure is modified from (S. Q. Liu et al., 2010).

factors of 5.5, 6.9 and 15.0 Å^2 for Asp39, His69 and Ser224, respectively. This is consistent with the unfavorable geometry of the Ser O_γ observed in some crystal structures of serine proteases (Dauter et al., 1991; Rypniewski et al., 1995). Functionally, the high flexibility of the serine hydroxyl allows it to adopt different orientations to suit the needs for proton transfer, nucleophilic attack and subsequent release of the cleaved peptide product.

6.3 Large concerted motions of proteinase K

The essential dynamics (ED) technique (Amadei et al., 1993; Balsera et al., 1996) is utilized to investigate large concerted motions of proteinase K. This method is based on the diagonalization of a covariance matrix built from atomic fluctuations in a MD trajectory. The central hypothesis of ED is that only a few eigenvectors with large corresponding eigenvalues are important for describing the overall internal motion of a protein. Fluctuations along the first few eigenvectors are mainly large concerted motions and can often be connected to the functional properties of proteins (Barrett & Noble, 2005; S. Q. Liu et al., 2007a; S. Q. Liu et al., 2008; Mello et al., 2002).

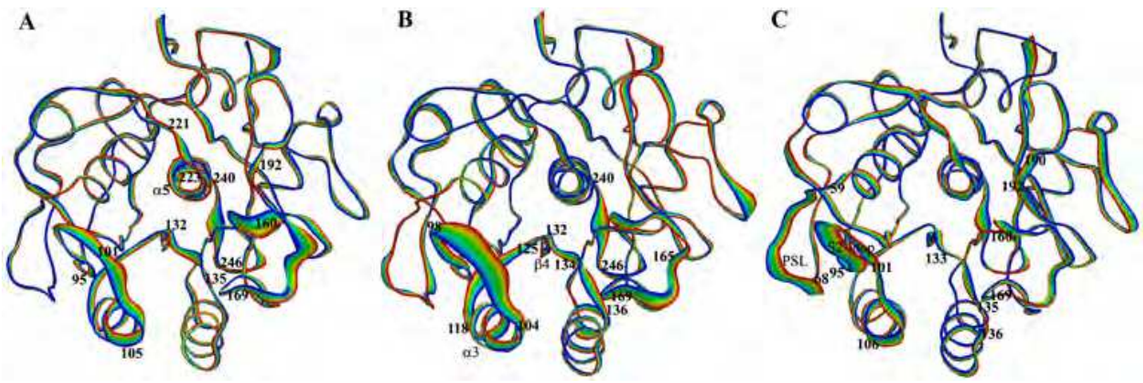

Fig. 8. The first three large concerted motions of proteinase K derived from essential dynamics analysis of the molecular dynamics simulation trajectory. (A) The most significant motion described by eigenvector 1, (B) Motion along eigenvector 2 and (C) motion along eigenvector 3. For each eigenvector, two extreme structures, which correspond to the largest and smallest projection values, respectively, were extracted from the eigenvector projection; and the intermediate frames were produced by simple interpolation between these two extremes. The linear interpolations between the two extremes are colored from blue to red to stress the structural differences between the two extremes but do not represent the transition pathway. This figure is modified from (S. Q. Liu et al., 2010).

For proteinase K, the large concerted motions described by the first three eigenvectors are shown in Figure 8. Visualization of motion along eigenvectors 1, 2 and 3 reveals that the structural changes originate mainly from displacements of the structural regions located within/around or opposite the substrate-binding site, i.e., residues100-105 (which are a part of the substrate-binding pocket S4), residues 118-125 (which are located opposite the S4 pocket), residues 160-169 and 221-223 (which are within the substrate-binding pocket S1), and residues 240-246 (which is located opposite the S1 pocket). The direct consequence of motions of the substrate-binding regions is dynamic variations of the substrate-binding pockets, i.e., the openings or closings of the S1 and S4 pockets, which may facilitate the binding/release of the peptide substrate/product into/out of the substrate-binding cleft.

Another interesting effect is that the large displacements in the regions located opposite or near the substrate-binding sites can mediate/modulate dynamics of substrate-binding regions. In the case of eigenvector 1, there are two segments containing residues 221-223 and 240-246 that exhibit large concerted displacements. As shown in Figure 8A, these two segments are separated by a helix α5 and lie opposite to each other. Since the α5 is rigid and shows only small fluctuation, we consider that it may act as the hinge region, allowing the large conformational displacements of segment 221-223 to be mediated by structural changes in the loop 240-246, suggesting that large concerted motions occurring in regions opposite the active Ser224 and S1 pocket can have effect on the dynamics of the active site. In the case of motions along eigenvector 2 (Figure 8B), a large displacement is observed in the loop region 118-125, which is located between the α3 following the substrate-binding residues 100-104 and the β4 preceding substrate-binding residues 132-136. Both α3 and β4 appear to be rigid and show small fluctuations, indicating that the dynamics of the substrate-binding segments 100-104 and 132-136 may be modulated by dynamic behavior of the opposite loop region containing residues 118-125. Here the rigid secondary structural elements linking the substrate-binding regions and the opposite loops may serve as hinge segments, allowing the transmission and communication of the conformational changes between these segments. In the case of eigenvector 3 (Figure 8C), an apparent large concerted motion is observed occurring between PSL (residues 59-68) and S2-loop (residues 95-101), which could, on the one hand, avoid steric clashes between these two loops because of their close locations in space; on the other hand, modulate the flexibility and orientation of the S2-loop, which, as described above (see section 4.5), plays a critical role in recognition and binding of the P2 and P3 residues of the substrate.

7. Substrate-induced change in molecular motions of proteinase K

In order further to investigate changes in dynamics of proteinase K upon the substrate binding, MD simulation of the structure of proteinase K in complex with the peptide substrate AAPA (Figure 6E; PDB code 3PRK (Wolf et al., 1991) was also performed (Tao et al., 2010). In this section, changes in molecular motions upon substrate binding and the dynamic behavior of substrate-binding pockets in the complexed proteinase K are examined. In addition, the functional implication of the changes in dynamics upon substrate binding and the mechanism underlying the conformational changes of substrate-binding regions are also discussed.

7.1 Changes in molecular motions of proteinase K upon substrate binding

Comparison of geometrical properties such as SASA, NNC, Rg and RMSD between the substrate-free and substrate-complexed proteinases K during MD simulations suggests that the enzyme structure is on average in a more compact and stable conformational state when the peptide substrate is present (data not shown; and for details see (Tao et al., 2010)).

Change in molecular motions of proteinase K upon substrate binding was investigated by using a method termed combined ED analysis. In this method, the MD trajectories of the free- and complexed-proteinases K were concatenated and the covariance matrix was constructed and diagonalized; the trajectories were then projected onto the combined eigenvectors and the properties of these projections were analyzed and compared. Figure 9A shows the comparison in the average values of the first 30 eigenvector projections between the two forms of proteinases K. The largest difference in the average of projection is

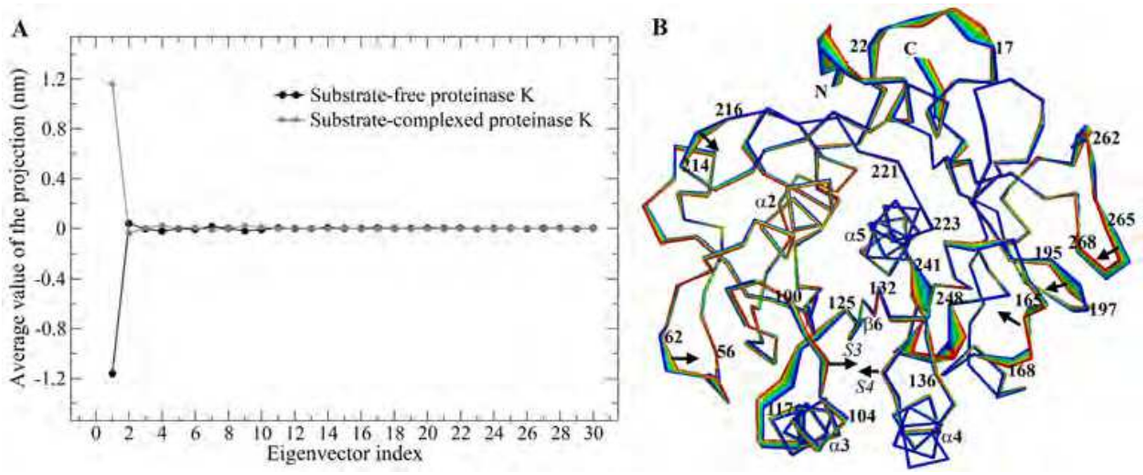

Fig. 9. Change in equilibrium conformation (molecular motion) of proteinase K upon substrate binding. (A) Comparison of the average values of projections of molecular dynamics simulation trajectories onto the combined eigenvectors as a function of eigenvector index. The substrate-free and substrate-complexed proteinase K trajectories were projected separately onto the combined eigenvectors followed by calculation of the average value of each projection. The values of the free and complexed proteinases K are indicated by black circles and grey squares, respectively. (B) The extreme structures extracted from the projection of the merged trajectory onto the first "combined" eigenvector. The linear interpolations between these two extremes are colored from blue (the free proteinase K) to red (the complexed proteinase K) to highlight the structural differences between these two states but do not represent the transition pathway. This figure is modified from (Tao et al., 2010).

observed between the first eigenvectors, indicating that the most significant change in molecular motions upon substrate binding is characterized by eigenvector 1. Similar or almost identical average values are observed for the eigenvectors with index greater than 2, suggesting that the molecular motions described by these eigenvectors are similar between these two states. Figure 9B shows that most of the structure exhibits minor conformational change upon substrate binding with the exception of the structural regions such as the N- and C-termini and some surface-exposed loops containing residues 56-62, 117-125, 162-168, 241-247 and 265-268, suggesting that substrate binding has only a minor influence on dynamics of the protein internal rigid core but a large effect on the external loops, in particular those located within or in the vicinity of the substrate binding site. Visualization of the motions along eigenvector 1 reveals that upon substrate binding, the large concerted motions originate mainly from displacements of residues 100-104 (which participate in the formation of the substrate-binding subsites S2-S4) and 165-168 (which are part of pocket S1), moving towards the peptide substrate leading to the closing of these substrate-binding pockets/sites. These are accompanied by motions of the surface-exposed loop residues 195-197 and 265-268 (which are located spatially close to residues 165-168) and 56-62 (which lie spatially adjacent to residues 100-104), moving concertedly to the direction of the substrate-binding groove resulting in the contractions of these surface loops. The most pronounced structural displacement upon substrate binding is observed in the loop composed of residues 241-248, which is located opposite the substrate-binding pocket S1 and connected to the surface-exposed loop residues 262-268 via helix α6. The small fluctuations of α6

indicate that the displacement of the segment 241-248 is capable of mediating structural change of the loop region 262-268, which in turn can modulate structural change of the loop residues 165-168 via the segment 195-197 to accommodate the C-terminal portion of the incoming substrate. Additionally, the displacement of the residues 241-248 also has an effect, similar to that observed in the substrate-free proteinase K, on dynamics of the segment 221-223. Another large displacement upon substrate binding is observed in the loop region comprising residues 117-125. Like also what is seen in the free proteinase K, the dynamic behavior of this loop can modulate the dynamics of the segments 100-104 and 132-136. Since the two segments 100-104 and 132-136 form the majority of the substrate-binding subsites/pockets S1-S4, their dynamic behaviors are of high importance in substrate recognition and binding and product release

7.2 Dynamic pockets of the substrate-complexed proteinase K

In the proteinase K-substrate complex, the large concerted motions of the substrate binding regions lead to the dynamic variations of the substrate-binding subsites/pockets,

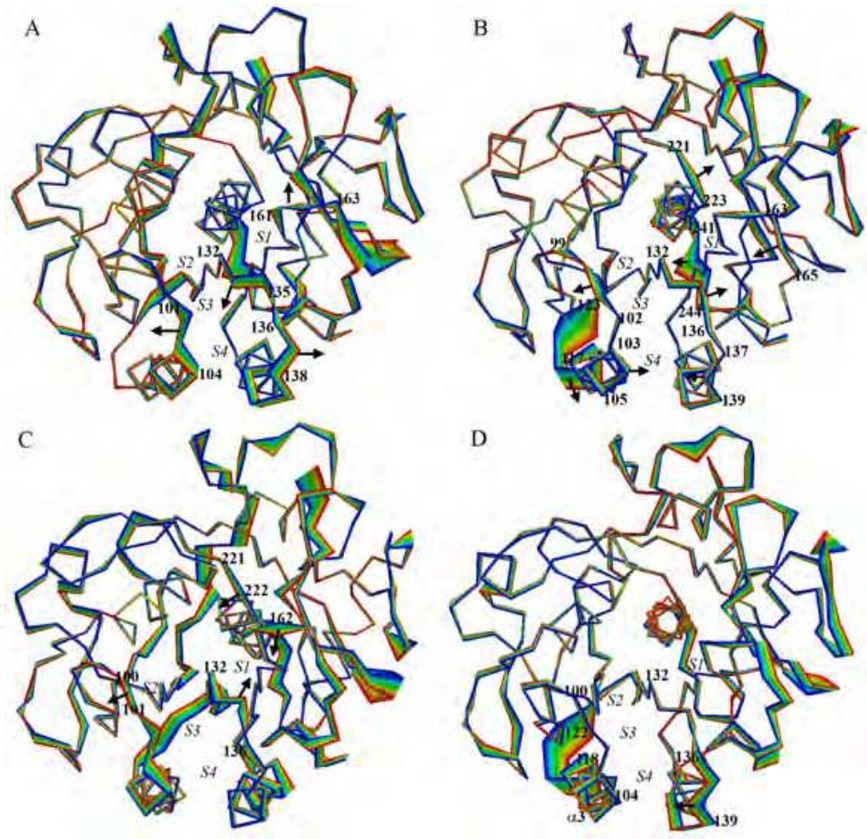

Fig. 10. The first four large concerted motions of the substrate-complexed proteinase K occurring along (A) eigenvector 1, (B) eigenvector 2, (C) eigenvector 3, and (D) eigenvector 4. The linear interpolations between the two extremes extracted from the projections of trajectory onto the first four eigenvectors are colored from blue to red to highlight the structural differences between them. The regions involving large concerted motions that cause dynamic variations of the substrate-binding pockets/subsites are labeled. This figure is modified from (Tao et al., 2010).

which are also observed in the free proteinase K as described in section 6.3. In the case of eigenvector 1, the concerted outward movements of the segments around S1 and S4 pockets, i.e., the segments 101-104 and 136-138 that form the two sides of the S4 pocket; and the segments 132-135 and 161-163 that form respectively the side and bottom of the S1 pocket, result in the enlargement of the these two pockets S1 and S4 (Figure 10A). In addition, the upper portion of the groove, where the subsites S2 and S3 reside, becomes narrowed due to the large inward displacement of the segment 132-134. In the case of eigenvector 2 (Figure 10B), loop 117-123 shows the largest downward displacement, which causes the segments 99-102 and 132-136 to move away from each other resulting in the opening of the upper portion of the binding groove. However, the lower portion of the binding groove (where the S4 pocket resides) becomes slightly narrowed due to the concerted inward movements of the segment 103-105 and 137-139. Simultaneously, the large leftward displacement of the segment 240-246 causes the segment 221-223 to move outwards, thus opening up the lid of the S1 pocket, while the inward movement of the segments 132-135 and 163-165 reduce the size of the bottom of the S1 pocket. The large concerted motions along eigenvector 3 lead to a twist of the binding groove and closure of the S1 pocket (Figure 10C). The obvious outward displacement of residues 100-101 widens the S2 subsite and provides more space for the P2 residue, Pro282. In the case of eigenvector 4 (Figure 10D), no apparent displacement is observed in segments of residues 100-104 and 132-136 whereas the largest displacement is observed in the segment 118-123, which mediates the segment 136-139 to move towards the helix α3, resulting in the reduction in size of the S4 pocket bottom. These complicated dynamic variations of the substrate-binding subsites/pockets reflect the rough free energy surface with several minima of the energy landscape of proteinase K, which can be related to dynamic catalytic processes of proteinase K and this, will be discussed below.

7.3 Functional implication of the dynamic pockets

In the case of the substrate-complexed proteinase K, the large concerted motions along the first eigenvector enlarge the pockets S1 and S4, providing more space for the P1 and P4 substrate residues for accommodation and subsequent orientation of them. The simultaneous closing of the subsites S2 and S3 could grip the corresponding substrate residues P2 and P3 to prevent release of the peptide substrate prior to catalysis. Because the motions along the eigenvector 2 lead to the opening of the lids and reduction of the bottoms of both S1 and S4 pockets, together with the opening of the upper portion (where the subsites S2 and S3 reside) of the binding groove, we may conclude that these motions possibly facilitate the substrate release. The twist motion of the binding groove along eigenvector 3 could facilitate the precise orientation of the P2-P4 residues. Interestingly, the observed closing of the S1 pocket in this subspace could be related to the precise positioning of the P1 substrate residue, a prerequisite for the nucleophilic attack to take place. Also worth noting is the approach of Ser224 to the P1 substrate residue, suggesting that this motional mode may be in the stage ready for the nucleophilic attack. The large concerted motions described by eigenvector 4 reduce the size of S4 pocket bottom and as such can be linked to the release of the S4 substrate residue. Among the first four motional modes, two modes, i.e., those along eigenvectors 2 and 4, lead to reduced size of the bottom of the S4 pocket, implying that the release of the cleaved C-terminal peptide product is possibly initiated by the dissociation of the P4 from the enzyme. In summary, the catalytic processes of the substrate binding, orientation, catalysis and product release occur at distinct modes of molecular flexibility, which correspond to different conformational substates located within

the wells of local free energy minima of the free energy landscape. The relatively small energy barriers between these minima allow the molecular motions and conformational transition to occur among them, thus realizing the catalytic function of the protease.

8. Difference in structural features between cuticle-degrading proteases secreted by nematode-parasitic and nematode-trapping fungi

8.1 Functional differences between alkaline and neutral cuticle-degrading proteases

The classical serine protease proteinase K and cuticle-degrading proteases such as PR1, VCP1, Ver112 and PL646 investigated above are all alkaline proteases because they work best in the pH range of 8 to 11. Another feature of alkaline proteases is that they show both high structural stability and high catalytic activity at high temperature, with a typical range of optimal reaction temperature of 50-60 °C. Interestingly, all the alkaline cuticle-degrading proteases that have been identified and characterized to date are secreted by nematode-parasitic fungi (J. Li et al., 2010), one type of nematophagous fungi that exist as conidia in the environment and infect nematodes by either adhering to the surface of the prey or by direct ingesting (X.Z. Liu et al., 2009). The conidia of the nematode-parasitic fungi can germinate rapidly and invade the entire nematode with assimilative hyphae absorbing all the body contents (Gray, 1987). Another type of nematophagous fungi is the nematode-trapping fungi, which can catch and hold actively the live nematodes using their trapping devices, i.e., the hyphal network, constricting rings and adhesive knobs that are formed by an extensive hyphal system (X.Z. Liu et al., 2009). The captured victim is then penetrated, with its entire body contents being consumed rapidly (Barron, 1977). During such a process, nematode-trapping fungi can also secrete enzymes to degrade the cuticle and body contents of the nematodes. Most of these enzymes were identified to be serine proteases, which, like those secreted by nematode-parasitic fungi, belong also to S8 peptidase family (Huang et al., 2004; J. K. Yang et al., 2007). Phylogenetic analysis of these serine proteases indicates that, despite belonging to the same family, they can be divided into two groups (Gray, 1987), i.e., the alkaline serine proteases derived from nematode-parasitic fungi and the neutral proteases derive from the nematode-trapping fungi. Compared to the alkaline serine proteases, the neutral cuticle-degrading proteases is optimally active at neutral pH and at relative low temperatures ranging from 30 to 40 °C. Furthermore, neutral protease exhibits relatively low structural stability and catalytic activity against nematode cuticle extract in comparison to alkaline protease (Liang et al., 2011).

Here in this section, we selected two cuticle-degrading proteases, i.e., Ver112 derived from nematode-parasitic fungus *L. psalliotae* and PII from nematode-trapping fungus *A. oligospora*, as representatives of the alkaline and neutral proteases, respectively, to identify structural factors responsible for different thermal stability and catalytic activity against nematode cuticle. The correlation between the electrostatic surface potential and phylogenetic relationship of alkaline and neutral proteases was investigated to probe the mechanism responsible for the distinct infectious virulence by different fungal species.

8.2 Structural comparison between Ver112 and PII

The amino acid sequence length of the alkaline protease Ver112 and neutral protease PII is 280 and 286, respectively; and the sequence identity between them is 46.6%. The three-dimensional structure of PII was modeled based on templates of the crystal structures of Ver112 (PDB code 3F7M (Liang et al., 2010)) and proteinase K (PDB code 1IC6) using

homology modeling software package MODELLER (Sali & Blundell, 1993). Because of their high degree of sequence identity, it is not surprising that the structural model of PII is highly similar to the crystal structure of Ver112, with backbone RMSD between them being ~ 0.65 Å. Their structural superposition shows that the structure core composed of the major secondary structure elements are well matched, while some surface-exposed turns and loops exhibiting relatively large structural deviations (Figure 11B). We consider that it is the highly conserved amino acids within the regions of secondary structure elements and more amino acid insertions and deletions in regions of loops/turns than in secondary structural regions that give rise to these differences. The catalytic triad Asp-His-Ser and oxyanion hole are conserved between proteases Ver112 and PII, either in sequence or structurally.

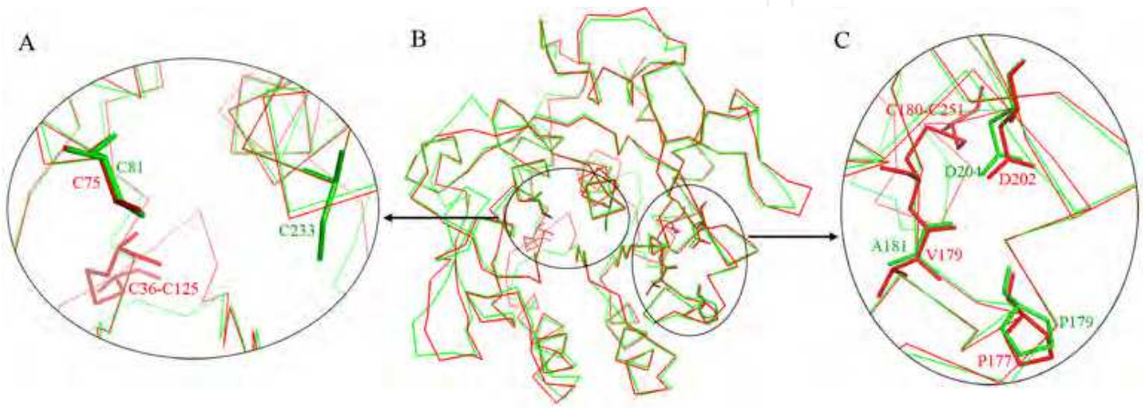

Fig. 11. Structural comparison between the experimentally determined crystal structure of Ver112 (PDB code 3F7M) and theoretically modeled structure of PII. (A, C) Locally enlarged structural regions showing disulfide bond, free cysteine and calcium binding site. The residues forming the disulfide bonds and Ca1 sites and the free cysteines are shown as stick models and labeled with red for Ver112 and green for PII. (B) The superposition of backbone of Ver112 (red) and PII (green).

The strong calcium cation Ca1 may also present in the structure of PII because of the presence of the Ca1 site residues (i.e., Pro179, Ala181 and Asp204 shown in Figure 11C) positionally equivalent to those in PL646 (PDB code 3F7O) and proteinase K (PDB code 1IC6), contributing to some extent to the stability of PII structure. However, the weak calcium cation Ca2 present in 1IC6 may not exist in PII due to the lack of equivalent Ca2 site residues.

As described in sections 4.2 and 4.3.2, the five completely conserved cysteines (at positions 34, 73, 123, 178 and 249; proteinase K numbering) among the alkaline proteases are predicted to form two disulfide bonds, i.e., Cys34-Cys123 and Cys178-Cys249, based on the homology models; and this is verified by the subsequently determined high-resolution crystal structure of Ver112 (PDB code 3F7M; Figure 11) as described in section 5.1, showing the presence of two disulfide bonds Cys36-Cys125 and Cys180-Cys251; and that the Cys75 is free. However, there is no cysteine found at the positions 34, 123, 178 and 249 (proteinase K numbering) in the neutral protease PII; and the disulfide bond can not be formed between the two mere cysteines Cys81 (equivalent to the free Cys73 in 1IC6 and free Cys75 in Ver112) and Cys233 in PII due to the large spatial separation between them (Figure 11A, B). Summarily, the alkaline protease Ver112 has two disulfide bonds, Cys36-C125 and C180-

C251 (Ver112 numbering) whereas the neutral protease PII contains no disulfide bond; and Ver112 displays higher thermal stability and stronger nematicidal/catalytic activity than PII does (Liang et al., 2011).

8.3 Role of disulfide bond in structural stability and flexibility

In order to investigate how the disulfide bonds influence structural stability and flexibility of these two proteases, MD simulations on their structures of wild-type and disulfide bond-disrupted mutant (Ver112_123C/A, Ver112_178C/A, and Ver112_123C/A_178C/A; proteinase K numbering) were performed at temperatures 300 K and 400 K, respectively. Analyses of the geometrical properties along the 300 K MD trajectories indicate that PII has higher average values of C_α RMSD and SASA while lower average values of NNH and NNC, suggesting a higher flexibility and less compact equilibrium structure of PII in comparison with Ver112. This may be caused by the lack of equivalent disulfide bonds in PII.

The geometrical properties of Ver112 are similar on average to those of its three mutants during MD simulations at 300 K, whereas at 400 K the wild-type Ver112 presents more NHB and NNC and less SASA than its mutants, suggesting that disulfide bonds contribute to the global stability of Ver112 at high temperature. Additionally, the stability of local structures within 5 Å of the two disulfide bonds Cys34-C123 and Cys178-Cys249 was also enhanced by disulfide bonds, as demonstrated by their increased RMSF and decreased NNC values in mutants with disrupted disulfide bonds compared to the wild-type structure. Analyses of the average RMSF values of the S1 and S4 substrate-binding pockets show that upon disruption of Cys34-Cys123, RMSF of S1 pocket decreased by 21.2% while that of S4 pocket showed almost no change; upon disruption of Cys178-Cys249, the relatively large reduction in flexibility of both S1 and S4 pockets was observed; and the most pronounced reduction (30.7% and 17.2%) was observed when both disulfide bonds were broken.

We can conclude based on these results: i) the presence of disulfide bonds enhances not only the local but also the global stability of the protease, thus explaining the higher thermal stability of the alkaline protease Ver112 compared to that of the neutral protease PII; ii) the presence of disulfide bonds increases the flexibility of substrate-binding pockets located relatively far from disulfide bonds, thus explaining why alkaline proteases have higher substrate affinity and catalytic activity (S. Q. Liu et al., 2011; Tao et al., 2010) than neutral proteases.

8.4 The correlation between electrostatic surface potential and phylogenetic relationship

Furthermore, the correlation between electrostatic surface potential and phylogenetic relationship of the available cuticle-degrading proteases were investigated. These include 14 neutral proteases derived from nematode-trapping fungi and four alkaline proteases from nematode-parasitic fungi. The amino acid sequences of the mature neutral proteases were obtained from GeneBank database with accession numbers/species sources of AB120125/*M.megalosporum,* AF516146 (Aoz1)/*A.oligospora,* AY859780/*M.cystosporum,* AY859781/*M.elegans,* AY859782/*A.Conoides,* DQ531603/*D.varietas,* EF055263/*A.multisecundaria,* EF113088/*A.Musiformis,* EF113089/*A.yunnanensis,* EF113090/*M.psychrophilum,* EF113091/*M.Coelobrochum,* EF113092/*D.shizishanna,* EF681769/*M.haptotylum,* X94121 (PII)/*A.oligospora*. The structural models of these 14 proteases were constructed using homology modeling method based on template structures

Ver112 (PDB code 3F7M) and proteinase K (PDB code 1IC6) as described before (Liang et al., 2011; S.Q. Liu et al., 2007b). The structures of the four alkaline proteases PR1 (GeneBank accession number AJ416695), VCP1 (AJ427460), Ver112 (AY692148) and PL646 (EF094858) were either determined by X-ray crystallographic technique (for Ver112 and PL646) (Liang et al., 2010) or modeled by homology modeling method (for PR1 and VCP1) (S.Q. Liu et al., 2007b). The electrostatic surface potentials of these 18 cuticle-degrading proteases were then calculated with the Poisson-Boltzmann method using Swiss-PdbViewer (Guex & Peitsch, 1997); the phylogenetic tree of these proteases was constructed with neighbor-joining (NJ) method using the MEGA program (Tamura et al., 2007); and finally each electrostatic surface potential plot of these proteases was placed corresponding to its branch in the phylogenetic tree (Figure 12).

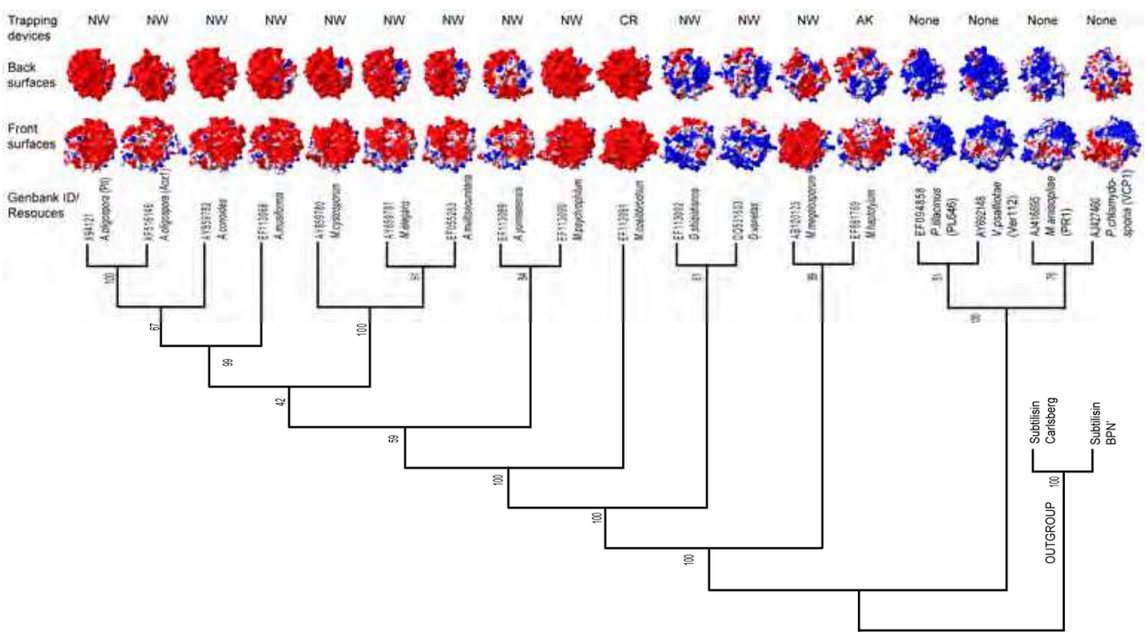

Fig. 12. Correlation between molecular electrostatic surface potentials of cuticle-degrading proteases and their phylogenetic relationship. The molecular electrostatic surfaces of these 18 proteases were calculated using Poisson-Boltzmann method and the phylogenetic tree was constructed using NJ method; and finally the electrostatic surface potential plots of each protease were placed at the position corresponding to its branch in the phylogenetic tree. Trapping devices of networks, constricting rings and adhesive knobs in the nematode-trapping fungi are abbreviated as NW, CR and AK, respectively. The nematode-parasitic fungi PL646, Ver112, PR1 and VCP1 contain no trapping device (None). Front surfaces are defined as molecular surfaces containing active site at its center; back surfaces are opposite to front surfaces. The positively and negatively charged electrostatic surfaces are colored blue and red, respectively. This figure is modified from (Liang et al., 2011).

Close inspection of Figure 12 reveals a good qualitative correlation between electrostatic surface potential and phylogenetic relationship of these proteases. Briefly, if proteases are phylogenetically more similar, they also exhibit more similar electrostatic potential distribution on the molecular surfaces, including both the front and back surfaces. For example, the neutral proteases PII and Aoz1 are clustered into the same small clade and

both exhibit overwhelming electro-negative potential distribution over all their protein surfaces. This can be interpreted by the highly similar amino acid sequence between these two proteases and the almost identical location of the equivalent amino acids in their three dimensional structures, leading to highly similar distribution of the partial charges between molecular surfaces of these two proteases. As expected, all the 14 neutral proteases derived from fungi possessing trap devices are grouped into one large clade; and the other four alkaline proteases derived from fungi without trap device form the another clade. A common feature of the neutral proteases is that they exhibit a predominant electro-negative potential distribution both on the front surface (except for EF113092 and DQ531603 located in the same branch) and on the back-side surface (except for EF113092 and DQ531603 in the same branch, and AB120125 and EF681769 in the same branch), while for the alkaline proteases their back surfaces are predominantly positively charged (except for AJ427460/VCP1) and their front surfaces display dual character of electrostatic potential distribution: the electro-negative potential (red color) is mainly concentrated around the surface of substrate-binding channel, and the other regions of the front surface are largely positively charged (blue color) or exhibit electro-neutrality (white color). As described and discussed in earlier section, the anionic feature of the substrate-binding regions is able to increase the local conformational flexibility of binding pockets/sites, which in turn facilitates substrate binding and even enhances catalytic efficiency of proteases. This may explain the maintenance of electro-negative potential around the substrate-binding groove surface of these proteases, in particular around that of the alkaline cuticle-degrading proteases with dominant positive charges. Interestingly, the dominant distribution of electro-positive potential on the surface of the alkaline proteases would undoubtedly increase efficiency of diffusion and subsequent adsorption of proteases to the negatively charged surface of nematode cuticle due to electrostatic attraction force between the oppositely charged proteases and the cuticle. On the contrary, the diffusion of the neutral proteases towards nematode cuticle seems to be suppressed due to the electrostatic repulsion between the heavily negatively charged proteases and the negatively charged cuticle. However, the diffusion of proteases towards the host cuticle is unlikely the bottleneck of infection by the nematode-trapping fungi because the active capture of the prey with trap devices makes it easy for the directly full contact between the prey and the proteases, and therefore the secreted neutral proteases can degrade the captured nematode "unhurriedly". We consider that the trap devices may eliminate the constraints faced by nematode-parasitic fungi and, with the aid of the traps, the nematode-trapping fungi's neutral cuticle-degrading proteases may be subjected to a low selective pressure, whereas the nematode-parasitic fungi have to evolve to produce more powerful alkaline proteases to acquire nutrients due to the lack of trap device (J. Li et al., 2010; Liang et al., 2011).

9. Conclusion

Because of their essential role in the breakdown of the cuticles of nematodes or insects, a thorough understanding of the structure-function relationship of the cuticle-degrading proteases is of crucial importance for improving infectious virulence of nematophagous fungi through engineering modifications, which will facilitate in turn the development and exploitation of various nematophagous fungi as effective bio-control agents against nematodes. Here in this chapter a number of cuticle-degrading proteases produced by different fungi were studied in detail in terms of physicochemical properties, structural

features, catalytic kinetics, structural dynamics and electrostatic surface potential-phylogeny relationship. The high degree of sequence identity among these proteases determines their very similar three-dimensional structures and their category to belong to the S8 peptidase family. A common feature of the cuticle-degrading serine proteases is their broad substrate specificity and high catalytic activity, allowing nematophagous fungi to utilize maximally different kinds of cuticle protein components to acquire nutrients. The overall structures of these proteases present a well-defined globular fold with high rigidity that is maintained by multiple structural factors such van der Waal contacts, hydrogen bonds, salt bridges, disulfide bonds, Ca^{2+} binding and aromatic ring stacking. It is the high rigidity of the overall structures that prevents the autolysis or proteolysis of the cuticle-degrading proteases. However, a certain degree of flexibility in some surface-exposed loops, especially those around the substrate-binding sites, is necessary and even crucial for substrate binding and enzyme turnover. Like almost all the other enzymes, the catalytic reaction of cuticle-degrading proteases can be considered to consist of the following consecutive dynamic steps: i) diffusion of the substrate to the entrance to the substrate-binding site; ii) initial contacts of the substrate with substrate-binding site; iii) rearrangement of the substrate at the binding site into its bound orientation which is ready for nucleophilic attack; iv) enzyme catalysis and the formation of tetrahedral complex; v) rearrangement of the cleaved substrate to be ready for release; and vi) product release. All these steps involve mutual conformational adaption of the enzyme and the substrate, which is facilitated by dynamic variation of substrate-binding sites/pockets resulting from either the large concerted motions of enzyme backbone or the small side chain rearrangements/rotations. Despite the highly similar sequences and structures among the cuticle-degrading serine proteases derived from different nematophagous fungi, they can be divided into two groups of neutral and alkaline proteases, which are produced by nematode-trapping fungi and nematode-parasitic fungi, respectively. The differences in optimal reaction temperature, thermal stability, electrostatic surface potential, substrate-binding affinity and catalytic activity among these proteases can be considered to be the consequence of the subtle differences in amino acid components of these proteases, particularly those located in the substrate-binding regions, resulting in the changes in local and/or global structural dynamics, distribution of partial charges and in architecture and hydrophathy of substrate-binding pockets. Our results also suggest that nematode-parasitic and nematode-trapping fungi have evolved to adopt different strategy to infect nematode as reflected by different properties of the secreted cuticle-degrading proteases.

10. Acknowledgement

Research described was supported by grants from National Natural Science Foundation of China (No. 30860011 and 31160181) and Yunnan province (2007PY-22), and by foundation for Key Teacher of Yunnan University.

11. References

Amadei, A.; Linssen, A.B.M. & Berendsen, H.J.C. (1993). Essential dynamics of proteins. *Proteins,* 17, 412-425.

Arnorsdottir, J.; Kristjansson, M.M. & Ficner, R. (2005). Crystal structure of a subtilisin-like serine proteinase from a psychrotrophic *Vibrio* species reveals structural aspects of cold adaptation. *Febs J,* 272, 832-845.

Bajorath, J.; Raghunathan, S.; Hinricks, W. & Saenger, W. (1989). Long-range structural changes in proteinase K triggered by calcium ion removal. *Nature,* 337, 481-484.

Baker, D. & Sali, A. (2001). Protein structure prediction and structural genomics. *Science,* 294, 93-96.

Balsera, M.A.; Wriggers, W.; Oono, Y. & Schulten, K. (1996). Principal component analysis and long time protein dynamics. *J Phys Chem,* 100, 2567-2572.

Barrett, C.P. & Noble, M.E. (2005). Molecular motions of human cyclin-dependent kinase 2. *J Biol Chem,* 280, 13993-14005.

Barron, G.L. (1977). The nematode-destroying fungi. In: *Topics in mycobiology,* pp. 1-140, Canadian Biological Publications, Guelph.

Betzel, C.; Pal, G.P.; Struck, M.; Jany, K.D. & Saenger, W. (1986). Active-site geometry of proteinase K: crystallographic study of its complex with a dipeptide chloromethyl ketone inhibitor. *FEBS Lett,* 197, 105-110.

Betzel, C.; Pal, G.P. & Saenger, W. (1988). Three dimensional structure of proteinase K at 0.15 nm resolution. *Eur J Biochem,* 178, 155-171.

Betzel, C.; Teplyakov, A.V.; Harutyunyan, E.H.; Saenger, W. & Wilson, K.S. (1990). Thermitase and proteinase K: a comparison of the refined three-dimensional structures of the native enzymes. *Protein Eng,* 3, 161-172.

Betzel, C.; Singh, T.P.; Visanji, M.; Peters, K.; Fittkau, S.; Saenger, W. & Wilson, K.S. (1993). Structure of the complex of proteinase K with a substrate analogue hexapeptide inhibitor at 2.2-A resolution. *J Biol Chem,* 268, 15854-15858.

Betzel, C.; Gourinath, S.; Kumar, P.; Kaur, P.; Perbandt, M.; Eschenburg, S. & Singh, T.P. (2001). Structure of a serine protease proteinase K from *Tritirachium album* limber at 0.98 Å resolution. *Biochemistry,* 40, 3080-3088.

Bidochka, M.J. & Khachatourians, G.G. (1994). Basic proteases of entomopathogenic fungi differ in their adsorption properties to insect cuticle. *J Invertebr Pathol,* 64, 26-32.

Birktoft, J.J. & Blow, D.M. (1972). Structure of alpha-chymotrypsin. *J Mol Biol,* l68, 187-240.

Blaxter, M.L.; Page, A.P.; Rudin, W. & Maizels, R.M. (1992). Nematode surface coats: actively evading immunity. *Parasitol Today,* 8, 243-247.

Blow, D.M. (1976). Structure and mechanism of chymotrypsin. *Acc Chem Res,* 9, 145-152.

Brendel, V.; Bucher, P.; Nourbakhsh, I.; Blaisdell, B.E. & Karlin, S. (1992). Methods and algorithms for statistical analysis of protein sequences. *Proc Natl Acad Sci USA,* 89, 2002-2006.

Cox, G.; Kusch, M. & Edgar, R. (1981). Cuticle of Caenorhabditis elegans: its isolation and partial characterization. *J Cell Biol,* 90, 7-17.

Dauter, Z.; Betzel, C.; Genov, N.; Pipon, N. & Wilson, K.S. (1991). Complex between the subtilisin from a mesophilic bacterium and the Leech inhibitor eglin-C. *Acta Cryst B,* 47, 707-730.

DelMar, E.; Largman, C.; Brodrick, J. & Geokas, M. (1979). A sensitive new substrate for chymotrypsin. *Anal. Biochem,* 99, 316–320.

Dodson, G. & Wlodawer, A. (1998). Catalytic triads and their relatives. *Trends Biochem Sci,* 23, 347-352.

Ebeling, W.; Hennrich, N.; Klockow, M.; Metz, H.; Orth, H.D. & Lang, H. (1974). Proteinase K from *Tritirachium album* limber. *Eur J Biochem,* 47, 91-97.

Estell, D.A.; Graycar, T.P.; Miller, J.V.; Powers, D.B.; Burnier, J.P.; Ng, P.G. & Wells, J.A. (1986). Probing steric and hydrophobic effects on enzyme interactions by protein engineering. *Science,* 233, 659-663.

Feenstra, K.A.; Hess, B. & Berendsen, H.J.C. (1999). Improving efficiency of large time-scale molecular dynamics simulations of hydrogen-rich systems. *J Comp Chem,* 20, 786-798.

Fiedler, Z. & Sosnowska, D. (2007). Nematophagous fungus *Paecilomyces lilacinus* (Thom) Samson is also a biological agent for control of greenhouse insects and mite pests. *BioControl,* 52, 547-558.

Gill, S.C. & von Hipple, P. (1989). Calculation of protein extinction coefficients from amino acid sequence data. *Anal Biochem,* 182, 319-326.

Goettel, M.S.; St Leger, R.J.; Rizzo, N.W.; Staples, R.C. & Roberts, D.W. (1989). Ultrastructural localization of a cuticle-degrading protease produced by the entomopathogenic fungus *Metarhizium anisopliae* during penetration of host (Manduca sexta) cuticle. *J Gen Microbiol,* 135, 2233-2239.

Gray, N.F. (1987). Nematophagous fungi with particular reference to their ecology. *Biol Rev,* 62, 245–304.

Gudjonsdottir, K. & Asgeirsson, B. (2008). Effects of replacing active site residues in a cold-active alkaline phosphatase with those found in its mesophilic counterpart from Escherichia coli. *Febs J,* 275, 117-127.

Guex, N. & Peitsch, M.C. (1997). SWISS-MODEL and the Swiss-PdbViewer: an environment for comparative protein modeling. *Electrophoresis,* 18, 2714-2723.

Helland, R.; Larsen, A.N.; Smalas, A.O. & Willassen, N.P. (2006). The 1.8 Å crystal structure of a proteinase K-like enzyme from a psychrotroph Serratia species. *Febs J,* 273, 61-71.

Hilz, H.; Wiegers, U. & Adamietz, P. (1975). Stimulation of proteinase K action by denaturing agents: application to the isolation of nucleic acids and the degradation of 'masked' proteins. *Eur J Biochem,* 56, 103-108.

Himmelhoch, S. & Zuckerman, B.M. (1978). Caenorhabditis briggsae: aging and the structural turnover of the outer cuticle surface and the intestine. *Exp Parasitol,* 45, 208-214.

Huang, X.W.; Zhao, N.H. & Zhang, K.Q. (2004). Extracellular enzymes serving as virulence factors in nematophagous fungi involved in infection of the host. *Res. Microbiol,* 155, 811-816.

Jansson, H.B. & Nordbring-Hertz, B. (1988). Infection mechanism in the fungus-nematode system. In: *Diseases of Nematodes*, G.J. Poinar, & H.B. Jansson, (Eds.), Vol. 2, pp. 59-72, CRC Press, Boca Raton Fla.

Jatala, P.; Kaltenbach, R. & Bocangel, M. (1979). Biological control of Meloidogyne incognita acrita and Globodera pallida on potatoes. *J Nematol,* 11, 303.

Jatala, P. (1986). Biological control of plant-parasitic nematodes. *Annu Rev Phytopathol,* 24, 453-489.

Joshi, L.; St Leger, R.J. & Bidochka, M.J. (1995). Cloning of a cuticle-degrading protease from the entomopathogenic fungus, *Beauveria bassiana*. *FEMS Microbiol Lett,* 125, 211-217.

Kabsch, W. & Sander, C. (1983). Dictionary of protein secondary structure: pattern recognition of hydrogen-bonded and geometrical features. *Biopolymers,* 22, 2577-2637.

Koshland, D.E.J. (1958). Application of a theory of enzyme specificity to protein synthesis. *Proc Natl Acad Sci USA,* 44, 98–104.

Kraut, J. (1977). Serine proteases: structure and mechanism of catalysis. *Ann Rev Biochem,* 46, 331-358.

Kumar, S. & Nussinov, R. (2004). Different roles of electrostatics in heat and in cold: adaptation by citrate synthase. *Chembiochem,* 5, 280-290.

Kyte, J. & Doolittle, R. (1982). A simple method for displaying the hydropathic character of a protein. *J Mol Biol,* 157, 105-132.

Lange, O.F.; Lakomek, N.A.; Fares, C.; Schroder, G.F.; Walter, K.F.A.; Becker, S.; Meiler, J.; Grubmuller, H.; Griesinger, C. & de Groot, B.L. (2008). Recognition dynamics up to microseconds revealed from an RDC-derived ubiquitin ensemble in solution. *Science,* 320, 1471-1475.

Lehninger, A.L. (1995). EMBL WWW Gateway to Isoelectric Point Service, In: *European Molecular Biology Laboratory,* Accessed Mar. 1, 2011, Available from: http://www.embl-heidelberg.de/cgi/pi-wrapper.pl

Li, J.; Yu, L.; Yang, J.K.; Dong, L.Q.; Tian, B.Y.; Yu, Z.F.; Liang, L.M.; Zhang, Y.; Wang, X. & Zhang, K. (2010). New insights into the evolution of subtilisin-like serine protease genes in Pezizomycotina. *BMC Evol Biol,* 10, 68.

Li, T.F.; Zhang, K.Q. & Liu, X.Z. (2000). *Taxonomy of nematophagous fungi*, Chinese Science and Technical Publishing, Beijing.

Liang, L.M.; Lou, Z.Y.; Ye, F.P.; Yang, J.K.; Liu, S.Q.; SunY.N; Guo, Y.; Mi, Q.L.; Huang, X.W.; Zou, C.G.; Meng, Z.H.; Rao, Z.H. & Zhang, K.Q. (2010). The crystal structures of two cuticle-degrading proteases from nematophagous fungi and their contribution to infection against nematodes. *Faseb J,* 24, 1391-1400.

Liang, L.M.; Liu, S.Q.; Yang, J.K.; Meng, Z.H.; Lei, L.P. & Zhang, K.Q. (2011). Comparison of homology models and crystal structures of cuticle-degrading proteases from nematophagous fungi: assessing the structural basis of nematicidal activity. *Faseb J,* Epub ahead of print. doi: 10.1096/fj.10-175653 fj.10-175653

Lindahl, E.; Hess, B. & van der Spoel, D. (2001). GROMACS 3.0: A package for molecular simulation and trajectory analysis. *J Mol Model,* 7, 306-317.

Liu, S.Q.; Liu, C.Q. & Fu, Y.X. (2007a). Molecular motions in HIV-1 gp120 mutants reveal their preferences for different conformations. *J Mol Graphics Modell,* 26, 306-318.

Liu, S.Q.; Meng, Z.H.; Yang, J.K.; Fu, Y.X. & Zhang, K.Q. (2007b). Characterizing structural features of cuticle-degrading proteases from fungi by molecular modeling. *BMC Struct Biol,* 7, 33.

Liu, S.Q.; Liu, S.X. & Fu, Y.X. (2008). Molecular Motions of Human HIV-1 gp120 Envelope Glycoproteins. *J Mol Model,* 14, 857-870.

Liu, S.Q.; Meng, Z.H.; Fu, Y.X. & Zhang, K.Q. (2010). Insights derived from molecular dynamics simulation into the molecular motions of serine protease proteinase K. *J Mol Model,* 16, 17-28.

Liu, S.Q.; Meng, Z.H.; Fu, Y.X. & Zhang, K.Q. (2011). The effect of calciums on the molecular motions of proteinase K. *J Mol Model,* 17, 289-300.

Liu, X.Z.; Xiang, M.C. & Che, Y.S. (2009). The living strategy of nematophagous fungi. *Mycoscience,* 50, 20-25.

Lobna, M. & Zawam, H. (2010). Efficacy of some biocontrol agents on reproduction and development of meloidogyne incognita infecting tomato. *Journal of American Science,* 6, 495-509.

Müller, A.; Hinrichs, W.; Wolf, W.M. & Saenger, W. (1994). Crystal structure of calcium-free proteinase K at 1.5-Å resolution. *J Biol Chem,* 269, 23108-23111.

Martin, J.R.; Mulder, F.A.A.; Karimi-Nejad, Y.; van der Zwan, J.; Mariani, M.; Schipper, D. & Boelens, R. (1997). The solution structure of serine protease PB92 from *bacillus alcalophilus*. *Structure,* 5, 521–532.

Matsumura, M.; Signor, G. & Matthews, B.W. (1989). Substantial increase of protein stability by multiple disulfide bonds. *Nature,* 342, 291-293.

Mello, L.V.; de Groot, B.L.; Li, S. & Jedrzejas, M.J. (2002). Structure and flexibility of Streptococcus agalactiae hyaluronate lyase complex with its substrate: insights into the mechanism of processive degradation of hyaluronan. *J Biol Chem,* 277, 36678-36688.

Monod, J.; Wyman, J. & Changeux, J.P. (1965). On the nature of allosteric transitions: a plausible model. *J Mol Biol,* 12, 88-118.

Morton, C.O.; Hirsch, P.R.; Peberdy, J.P. & Kerry, B.R. (2003). Cloning of and genetic variation in protease VCP1 from the nematophagous fungus *Pochonia chlamydosporia*. *Mycol Res,* 107, 38-46.

Moult, J.; Sussman, F. & James, M.N.G. (1985). Electron density calculations as an extension of protein structure refinement: SGPA at 1.5 Å resolution. *J Mol Biol,* 182, 555-566.

Murrell, K.D.; Graham, C.E. & McGreevy, M. (1983). Strongyloides ratti and Trichinella spiralis: net charge of epicuticle. *Exp Parasitol,* 55, 331-339.

Nishihira, J. & Tachikawa, H. (1996). Theoretical evaluation of a model of the catalytic triads of serine and cysteine proteases by ab initio molecular orbital calculation. *J Theor Biol,* 196, 513-519.

Niu, Q.H.; Huang, X.W.; Zhang, L.; Xu, J.P.; Yang, D.M.; Wei, K.B.; Niu, X.M.; An, Z.Q.; Bennett, J.W.; Zou, C.G.; Yang, J.K. & Zhang, K.Q. (2010). A Trojan horse mechanism of bacterial pathogenesis against nematodes. *Proc Natl Acad Sci USA,* 107, 16631-16636.

Nordbring-Hertz, B. (2004). Morphogenesis in the nematode-trapping fungus Arthrobotrys oligospora: an extensive plasticity of infection structures. *Mycologist,* 18, 125-133.

Page, A.P. & Johnstone, I.L. (2007). The cuticle. In: *WormBook*, J.M. Kramer, & D.G. Moerman, (Eds.), The *C. elegans* Research Community, WormBook, doi/10.1895/wormbook.1.138.1.

Pahler, A.; Banerjee, A.; Dattagupta, J.K.; Fujiwara, T.; Lindner, K.; Pal, G.P.; Suck, D. & Saenger, W. (1984). Three-dimensional structure of fungal proteinase K reveals similarity to bacterial subtilisin. *Embo J,* 3, 1311-1314.

Pasternak, A.; Ringe, D. & Hedstrom, L. (1999). Comparison of anionic and cationic trypsinogens: the anionic activation domain is more flexible in solution and differs in its mode of BPTI binding in the crystal structure. *Protein Sci,* 8, 253-258.

Perica, T. & Chothia, C. (2010). Ubiquitin - molecular mechanisms for recognition of different structures. *Curr Opin Struct Biol,* 20, 367-376.

Rawlings, N.D.; Barrett, A.J. & Bateman, A. (2010). MEROPS: the peptidase database. *Nucleic Acids Res,* 38, D227-D233.

Rombach, M.C.; Aguda, R.M.; Shepard, B.M. & Roberts, D.W. (1986). Infection of rice brown planthopper, Nilaparvata lugens (Homoptera: Delphacidae), by field application of entomopathogenic hyphomycetes (Deuteromycotina). *Environ Entomol,* 15, 1070-1073.

Russell, A.J. & Fersht, A.R. (1987). Rational modification of enzyme catalysis by engineering surface charge. *Nature,* 328, 496-500.

Rypniewski, W.R.; Dambmann, C.; von der Osten, C.; Dauter, M. & Wilson, K.S. (1995). Structure of inhibited trypsin from *Fusarium oxysporum* at 1.55 Å. *Acta Cryst D,* 51, 73-84.

Saberhagen, C.; Klotz, S.A.; Bartholomew, W.; Drews, D. & Dixon, A. (1997). Infection due to *Paecilomyces lilacinus*: a challenging clinical identification. *Clin Infect Dis,* 25, 1411-1413.

Sali, A. & Blundell, T.L. (1993). Comparative protein modelling by satisfaction of spatial restraints. *J Mol Biol,* 234, 779-815.

Sasser, J. & Freekman, D. (1987). A world perspective on nematology: the role of the society. In: *Vistas on Nematology*, J.A. Veech, & D.W. Dickson, (Eds.), Society of Nematologists, Hyattsville, MD, USA.

Schmitt, D.P. & Sipes, B.S. (1998). *Plant-parasitic nematodes and their management*. Cooperative extension service, college of tropical agriculture and human resources, University of Hawaii at Manoa, Retrieved from http://www.ctahr.hawaii.edu/oc/freepubs/pdf/PD-15.pdf

Segers, R.; Butt, T.; Kerry, B. & Peberdy, J. (1994). The nematophagous fungus *Verticillium chlamydosporium* produces a chymoelastase-like protease which hydrolyses host nematode proteins in situ. *Microbiology,* 140, 2715-2723.

Segers, R.; Butt, T.M.; Kerry, B.R.; Beckett, A. & Peberdy, J.F. (1996). The role of the proteinase VCP1 produced by the nematophagous *Verticillium chlamydosporium* in the infection process of nematode eggs. *Mycol Res,* 100, 421-428.

Sevier, C.S. & Kaiser, C.A. (2002). Formation and transfer of disulphide bonds in living cells. *Nat Rev Mol Cell Biol,* 3, 836-847.

Shirley, B.A.; Stanssens, P.; Hahn, U. & Pace, C.N. (1992). Contribution of hydrogen bonding to the conformational stability of ribonuclease T1. *Biochemistry,* 31, 725-732.

Siezen, R.J.; de Vos, W.M.; Leunissen, J.A. & Dijkstra, B.W. (1991). Homology modelling and protein engineering strategy of subtilases, the family of subtilisin-like serine proteinases. *Protein Eng,* 4, 719-737.

Siezen, R.J. & Leunissen, J.A.M. (1997). Subtilases: the superfamily of subtilisin-like serine proteases. *Protein Sci,* 6, 501-523.

Snyder, D. (2002). Plant parasitic nematodes-an introduction, In: *North Crolina State University,* Accessed Mar. 10, 2011, Available from: http://www.cals.ncsu.edu/pgg/dan_webpage/index.htm

St Leger, R.J.; Cooper, R.M. & Charnley, A.K. (1986). Cuticle-degrading enzymes of entomopathogenic fungi: degradation in vitro by enzymes from entomopathogens. *J Invertebr Pathol,* 48, 167-177.

St Leger, R.J.; Charnley, A.K. & Cooper, R.M. (1987). Characterization of cuticle-degrading proteases produced by the entomopathogen *Metarhizium anisopliae*. *Arch Biochem Biophys,* 253, 221-232.

St Leger, R.J.; Frank, D.C.; Roberts, D.W. & Staples, R.C. (1993). Molecular cloning and regulatory analysis of the cuticle degrading protease structural gene from the entomopathogenic fungus *Metarhizium anisopliae*. *Eur J Biochem,* 204, 991-1001.

Stirling, G.R. & West, L.M. (1991). Fungal parasites of root-knot nematode eggs from tropical and sub-tropical regions of Australia. *Australas Plant Path,* 20, 149-154.

Tamura, K.; Dudley, J.; Nei, M. & Kumar, S. (2007). MEGA4: molecular evolutionary genetics analysis (MEGA) software version 4.0. *Mol Biol Evol,* 24, 1596-1599.

Tao, Y.; Rao, Z.H. & Liu, S.Q. (2010). Insight derived from molecular dynamics simulation into substrate-induced changes in protein motions of proteinase K. *J Biomol Struct Dyn,* 28, 143-157.

Teplyakov, A.V.; Kuranova, I.P.; Harutyunyan, E.H.; Vainstein, B.K.; Frommel, C.; Hohne, W.E. & Wilson, K.S. (1990). Crystal structure of thermitase at 1.4 Å. *J Mol Biol,* 214, 261-279.

Tian, B.; Yang, J.K. & Zhang, K.Q. (2007). Bacteria used in the biological control of plant-parasitic nematodes: populations, mechanisms of action and future prospects. *FEMS Microbiol Ecol,* 61, 197-213.

Tobi, D. & Bahar, I. (2005). Structural changes involved in protein folding correlate with intrinsic motions of proteins in the unbound state. *Proc Natl Acad Sci USA,* 102, 18908-18913.

Tsukuda, H. & Blow, D.M. (1985). Structure of alpha-chymotrypsin refined at 1.68 Å resolution. *J Mol Biol,* 184, 703-711.

Tunlid, A.; Rosen, S.; Ek, B. & Rask, L. (1994). Purification and characterization of an extracellular serine protease from the nematode-trapping fungus Arthrobotrys oligospora. *Microbiology,* 140, 1687-1695.

Wells, J.A.; Powers, D.B.; Bott, R.R.; Graycar, T.P. & Estell, D.A. (1987). Designing substrate specificity by protein engineering of electrostatic interactions. *Proc Natl Acad Sci USA,* 84, 1219-1223.

Westenfeld, F.; Alston, W.K. & Winn, W.C. (1996). Complicated soft tissue infection with prepatellar bursitis caused by *Paecilomyces lilacinus* in an immunocompetent host: case report and review. *J Clin Microbiol,* 34, 1559-1562.

Wolf, W.M.; Bajorath, J.; Müller, A.; Raghunathan, S.; Singh, T.P.; Hinrichs, W. & Saenger, W. (1991). Inhibition of proteinase K by methoxysuccinyl-Ala-Ala-Pro-Ala-chloromethyl ketone: an X-ray study at 2.2-Å resolution. *J Biol Chem,* 266, 17695-17699.

Writing, A. (2011). The advantages of biological pest control, In: *ehow.com,* Accessed Mar. 12, 2011, Available from: http://www.ehow.com/list_5985349_advantages-biological-pest-control.html

Yang, J.K.; Huang, X.W.; Tian, B.Y.; Sun, H.; Duan, J.X.; Wu, W.P. & Zhang, K.Q. (2005a). Characterization of an extracellular serine protease gene from the nematophagous fungus *Lecanicillium psalliotae*. *Biotechnol Lett,* 27, 1329-1334.

Yang, J.K.; Huang, X.W.; Tian, B.Y.; Wang, M.; Niu, Q.H. & Zhang, K.Q. (2005b). Isolation and characterization of a serine protease from the nematophagous fungus, *Lecanicillium psalliotae*, displaying nematicidal activity. *Biotechnol Lett,* 27, 1123-1128.

Yang, J.K.; Tian, B.Y.; Liang, L.M. & Zhang, K.Q. (2007). Extracellular enzymes and the pathogenesis of nematophagous fungi. *Appl Microbiol Biotechnol,* 75, 21-31.

Yang, J.K.; Wang, L.; Ji, X.L.; Feng, Y.; Li, X.M.; Zou, C.G.; Xu, J.P.; Ren, Y.; Mi, Q.L.; Wu, J.L.; Liu, S.Q.; Liu, Y.; Huang, X.W.; Wang, H.Y.; Niu, X.M.; Li, J.; Liang, L.M.; Ji, K.F.; Zhou, W.; Yu, Z.F.; Li, G.H.; Liu, Y.J.; Li, L.; Qiao, M.; Feng, L. & Zhang, K.Q. (2011). Genomic and proteomic analyses of the fungus Arthrobotrys oligospora provide insights into nematode-trap formation. *Plos Pathog,* submitted.

Zhao, M.L.; Mo, M.H. & Zhang, K.Q. (2004). Characterization of a neutral serine protease and its full-length cDNA from the nematode-trapping fungus *Arthrobotrys oligospora*. *Mycologia,* 96, 16-22.

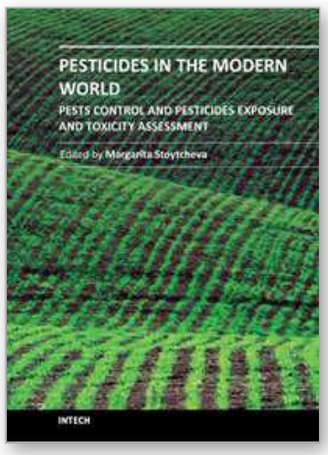

Pesticides in the Modern World - Pests Control and Pesticides Exposure and Toxicity Assessment

Edited by Dr. Margarita Stoytcheva

ISBN 978-953-307-457-3
Hard cover, 614 pages
Publisher InTech
Published online 30, September, 2011
Published in print edition September, 2011

The present book is a collection of selected original research articles and reviews providing adequate and up-to-date information related to pesticides control, assessment, and toxicity. The first section covers a large spectrum of issues associated with the ecological, molecular, and biotechnological approaches to the understanding of the biological control, the mechanism of the biocontrol agents action, and the related effects. Second section provides recent information on biomarkers currently used to evaluate pesticide exposure, effects, and genetic susceptibility of a number of organisms. Some antioxidant enzymes and vitamins as biochemical markers for pesticide toxicity are examined. The inhibition of the cholinesterases as a specific biomarker for organophosphate and carbamate pesticides is commented, too. The third book section addresses to a variety of pesticides toxic effects and related issues including: the molecular mechanisms involved in pesticides-induced toxicity, fish histopathological, physiological, and DNA changes provoked by pesticides exposure, anticoagulant rodenticides mode of action, the potential of the cholinesterase inhibiting organophosphorus and carbamate pesticides, the effects of pesticides on bumblebee, spiders and scorpions, the metabolic fate of the pesticide-derived aromatic amines, etc.

INTECH
open science | open minds

InTech Europe
University Campus STeP Ri
Slavka Krautzeka 83/A
51000 Rijeka, Croatia
Phone: +385 (51) 770 447

InTech China
Unit 405, Office Block, Hotel Equatorial Shanghai
No.65, Yan An Road (West), Shanghai, 200040, China
中国上海市延安西路65号上海国际贵都大饭店办公楼405单元
Phone: +86-21-62489820

Fax: +385 (51) 686 166
www.intechopen.com

Fax: +86-21-62489821

IntechOpen